NOAA Technical Memorandum ERL ETL-258

5-mm RADIOMETRIC MEASUREMENTS FROM FLIP DURING COPE: A DATA SUMMARY

Y.G. Trokhimovski
E.R. Westwater
V.G. Irisov
V.Y. Leuskiy

Environmental Technology Laboratory
Boulder, Colorado
November 1995

noaa NATIONAL OCEANIC AND ATMOSPHERIC ADMINISTRATION / Environmental Research Laboratories

NOAA Technical Memorandum ERL ETL-258

5-mm RADIOMETRIC MEASUREMENTS FROM FLIP DURING COPE: A DATA SUMMARY

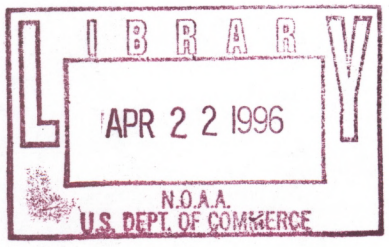

Yuri G. Trokhimovski
NRC Resident Associate
Environmental Technology Laboratory

Ed R. Westwater
Vladimir G. Irisov
Cooperative Institute for Research in Environmental Sciences (CIRES)
The University of Colorado/NOAA

Vladimir Ye. Lueskiy
Astro Space Center of the Lebedev Physical Institute
Russian Academy of Sciences, Moscow

Environmental Technology Laboratory
Boulder, Colorado
November 1995

UNITED STATES DEPARTMENT OF COMMERCE

Ronald H. Brown
Secretary

NATIONAL OCEANIC AND ATMOSPHERIC ADMINISTRATION

D. JAMES BAKER
Under Secretary for Oceans and Atmosphere/Administrator

Environmental Research Laboratories

James L. Rasmussen
Director

NOTICE

Mention of a commercial company or product does not consitute an endorsement by NOAA/ERL. Use for publicity or advertising purposes, or information from this publication or concerning proprietary products or the tests of such products is not authorized.

For sale by the National Technical Information Service, 5285 Port Royal Road, Springfield, VA 22061

CONTENTS

5-mm Radiometric Measurements from FLIP during COPE: a Data Summary

Yuri G. Trokhimovski[1], Ed R. Westwater[2], Vladimir G. Irisov[2], Vladimir Ye. Leuskiy[3]

ABSTRACT. Data obtained from a scanning 5-mm microwave radiometer during the Coastal Oceans Probing Experiment are presented. This instrument was deployed from the ocean platform FLIP, and from the radiometric data air/sea temperature difference and low altitude temperature profiles are derived.

1. INTRODUCTION

During September-October in 1995, the Environmental Technology Laboratory (ETL) conducted the Coastal Oceans Probing Experiment COPE off the Oregon coast. During this experiment, a 5-mm scanning radiometer was deployed on the research vessel FLIP. The instrument is designed for precise continuous measurements of air-water temperature difference and for recovery of air temperature profiles (h = 0-300 m). This device was first used from a research vessel during the Joint US-Russia Internal Waves Experiment in July 1992 (Trokhimovski et al., 1995a; Trokhimovski and Leuskiy, 1993; Trokhimovski et al, 1995b). The microwave part of the radiometer was designed and developed at the P. N. Lebedev Physical Institute in Moscow by Vladimir Leuskiy and the data acquisition system , which is an essential part of radiometer, was developed by Vladimir Irisov in ETL/NOAA , Boulder.

The main idea of the technique is to measure oceanic and atmospheric emission in a wavelength band that exhibits relatively high atmospheric attenuation. In this case, the radiation in the horizontal direction can be used as a reference level since the brightness temperature is equal to the air temperature at the measurement height. Radiometric measurements are made in a scanning mode and the radiometer measures brightness temperature relative to the air temperature. The radiometer is a total power system with automatic compensation of the direct current in the output signal (a compensation-type radiometer). No additional modulation except

---

[1]NRC Resident Associate, Environmental Technology Laboratory, Boulder, Colorado.

[2]Cooperative Institute for Research in Environmental Sciences, University of Colorado/NOAA, Boulder, Colorado.

[3]Astro Space Center of the Lebedev Physical Institute, Russian Academy of Sciences, Moscow, Russia.

the antenna beam rotation is done in the radiometer.

We have used radiometric measurements at wavelengths in the 5 mm oxygen absorption band. This wavelength band is usually employed for recovery of atmospheric temperature profiles (Westwater et al., 1975; Westwater, 1993). The same technique can be used at infrared or short millimeter wavelengths. The COPE data presented below have confirmed that, using 12-min averages, the technique recovers air-water temperature difference to an accuracy of about 0.1 K (or 5-7%) and that the instrument can provide long, continuous observations. The scanning radiometer is simple and can be used not only from a ship but also from low-altitude airborne platforms.

In addition to the water-air temperature difference, the same measurements provide information about air temperature profiles in the low atmosphere. Thus it is possible to compare different parameters which are related to heat and momentum fluxes and to check predictions of surface layer models. We suggest that the proposed technique could be deployed widely in the investigation of ocean - atmosphere interactions.

During COPE, 5-mm radiometric measurements were performed with an instrument slightly modified from the one used during JUSREX. First, the local oscillator in the radiometer was shifted to higher frequencies. The total band was estimated as 58.5 - 62.5 GHz. Note that this shift of central frequency does not change the skin depth, which is still 0.3 mm. Next, the polarization of radiometer was changed. During COPE the antenna received horizontal polarization (in JUSREX - vertical polarization). Near nadir, the water surface was observed at vertical polarization, at grazing angles, at horizontal polarization. Such an installation provides better agreement between air temperature and brightness temperature in the horizontal direction.

The use of the 5-mm radiometer in COPE required completion of a variety of tasks, including preparation of the radiometer, it's calibration, and development of a new data acquisition system. Below we summarize these 1995 activities:
1. May-June: V. Leuskiy prepared the 5-mm radiometer for COPE measurements. He exchanged the local oscillator for a new one with a center frequency of 60.5 GHz (Moscow).
2. May-June: V. Irisov developed a new QNX data acquisition system synchronized by control pulses from the radiometer (Boulder).
3. August 10-14: V.Irisov, V.Leuskiy, E. Westwater and Yu. Trokhimovski tested the 5-mm radiometer and new data acquisition system on the roof of the building occupied by ETL (Boulder).
4. August 18-19: V.Irisov, E. Westwater, Yu. Trokhimovski, Y. Han and Catherine Russell calibrated the radiometer at the ETL's Boulder Atmospheric Observatory, a 300-m research tower (Boulder).
5. August 25-31: J.Shaw and Yu. Trokhimovski installed the radiometer's computers in a rack on FLIP and did final testing (San Diego).
6. September 12 - September 24: J. Shaw installed the 5-mm radiometer on the south side of the port boom and conducted the radiometric measurements (FLIP).

7. September 25 - September 27: M. Jacobson conducted the radiometric measurements and prepared the radiometer for return transportation to ETL (FLIP).
8. October 10 - November 5: E. Westwater, V. Irisov and Yu. Trokhimovski analyzed 5-mm data (Boulder).

2. ROOF TESTING AND TOWER CALIBRATION

Initial measurements were conducted on August 10-14, 1995, on the roof of the 6-story building occupied by ETL and demonstrated that the radiometer worked well with new data acquisition system. It was noted that the speed of rotation of the scanning mirror varied slightly with time and for that reason the decision was made to increase the duration of one registration period to provide constant control of rotation speed. It was decided that the registration system would average every 10 scans in two domains. Roof testing also demonstrated that the coefficient of amplification increases rapidly if the air temperature becomes higher then 32° C.

The calibration of the radiometer output and antenna beam orientation was performed on the Boulder Atmospheric Observatory research tower (see Fig. 1) during August 18-19. Scale calibration was performed from different tower altitudes: 10,50,100,200 and 300 m. Brightness temperatures obtained as a function of angle calculated from horizon are shown in Fig. 2. Radiometric measurements were accompanied by radiosonde measurements and direct measurement of air temperature from tower platform. Radiosonde data and radiometric measurements from the heights 200 and 300 m were determined as the best for radiometer calibration. Brightness temperature was calculated using Liebes' model for absorption coefficients. The comparisons between measured and calculated profiles are shown in Figs. 3 and 4. We determined the following values for the calibration coefficient k ($T_b = a + k \cdot Y$, where Y is output counts of the registration system):

August 18,1995:
h =200 m, k=0.000388322,
h =300 m, k=0.000392136,
August 18,1995:
h =200 m, k=0.000394412
h =300 m, k=0.000420940

The mean value of the calibration coefficient $\langle k \rangle$ was calculated as **0.0003987**. This value was used for the COPE data analysis.

The angular calibration was done using a fluorescent lamp at distance about 10 m from the mirror. Fig. 5a shows the radiometric output when the lamp was sequentially turned on and off. Fig. 5b shows the lamp signal after subtracting the background brightness temperature. Measurements were done using an antenna with a main beam width of 6.6 degrees at the 3-dB level but as shown in Fig. 5 the width of signal is somewhat larger because the lamp can not be considered as a point source.

3. RESULTS OBTAINED FROM FLIP

The 5-mm radiometer was mounted on the south side of the port boom at a distance about 10 m from FLIP's main structure. The altitude of the radiometer relative to the water surface was about 6 m. On the same boom were located the fluxes package of Chris Fairall (ETL/NOAA) and instrumentation of APL/University of Washington (including W. Keller's scatterometer and . Jessup's infrared radiometers). In Fig. 6 the microwave and control units of the 5-mm scanning radiometer are presented and Fig. 7 shows the view of FLIP from a blimp that was operated during COPE. The port boom with the 5-mm radiometer is on the left side of the picture.

One example showing two angular cycles of the initial data is given in Fig. 8. The output values are plotted as a function of the number of the points (representing angles) of the output file. First we observe a large signal from supporting bulk, next, the signal of the internal noise generator (used for estimation of the stability of the calibration coefficient), and then the signal from the water surface, horizon, and atmosphere. The minimum of brightness temperature corresponds to the zenith observation. The high frequency variable signal at 260-360 corresponds to the multiple reflections caused by APL/UW equipment mounted at the same boom and from the boom itself.

The next twelve figures (Figs. 9 - 20) show calibrated and averaged examples of data for each day of the COPE. A constant offset has been subtracted from all of these data. We selected UTC: 0-1, 6-7, 12-13 and 18-19 for data averaging. Data are shown for the angle intervals 43-250 degree from nadir. For every two scans the rotation speed was determined using a correlation technique and a corresponding correction was applied to the values of angles. We also checked the value of internal noise generator (internal calibration) and concluded that within an accuracy of about 5-7 % it is possible to neglect all variations of the amplifier coefficient.

From visual inspection of the scans presented in Figs. 9 -20 it is possible get qualitative information about stability conditions. For example the maximum at zenith on September 23 is a direct indication of strong surface-based inversion in the atmosphere indicating stable conditions. On some scans we note, especially near zenith, the influence of ropes and cables supporting the boom.

Preliminary retrievals of air-water temperature were based on the brightness temperature measurements at angles 48-57 degree from nadir and with an averaging time of 12 min. The results are shown in Fig. 21. It can be noted that during COPE both stable and unstable condition were observed. The next figure (Fig. 22) shows for comparison in situ measurements performed by C. Fairall. Note that we show here air-water temperature differences based on preliminary in situ measurements and that in a final version some correction of the data will be made. Nevertheless we consider common agreement between in situ and 5-mm data as very good.

Ropes near zenith above radiometer made difficult the retrieval of air temperature profiles at high altitudes but fortuitously, the retrieval of temperature gradient in the layer 0-150 meters is based mainly on brightness temperature at small grazing angles (smaller then 45 degrees). Thus the measured data can be used also for retrieval of air temperature profiles (relative to air temperature near the sea surface). This part of analysis will be performed soon. Figs. 23 and 24 show an illustration of brightness temperature dependence near the horizon. At a first approximation the angular gradients of brightness temperature, which are shown in Figs. 23 and 24, are proportional to the air temperature gradient in the lower atmosphere. These measurements correlate well with air-water temperatures derived from the down-looking part of 5-mm measurements (Fig.21) and with in situ measurements (Fig.22).

An averaging time of 12 min is not necessary for a stable solution of the inverse problem. This time was used only to provide about the same time resolution with in situ measurements. The next step in data analysis was done for date averaged over 36.29 seconds. Figs. 25 - 48 show the obtained air-water temperature difference. Each figure represents 12 hours of measurements. The results indicate that intensity of the variability of the air-water temperature difference is large under stable atmospheric conditions! This may occur because of the wind flow from shore to FLIP during periods of stable stratification. Fig. 49 shows the square root of the variance of $\Delta=T_w - T_a$ for the high frequency part of spectrum. The original data were filtered in a such way that all variation with periods more that 1 hour were removed. It is seen that during stable conditions the variance is essentially higher than during unstable ones. The next figure (Fig.50) compares the spectral density of Δ under stable and unstable conditions. We have used the Julian Day time intervals 261.6 - 263.3(Fig.50a), 263.8 - 265.5 (Fig.50b), and 266.8 - 268.5 (Fig.50c). Each spectrum was calculated using a 10.3 h data set. The spectral density E(f) is normalized so, that $\sigma^2 = \Sigma (\Delta_i - <\Delta>)^2 /N= \int E(f)\, 2\pi\, df$, where f is the frequency in h^{-1} and the integration is made from 0 to ∞. Fig. 51 shows averaged spectra for the same time intervals.

We summarize our initial 60 GHz radiometric results:

a) Our 5-mm radiometer operated continuously about 12 days during COPE except for two gaps in time on September 17, Julian day 260 (radiometer was shut down because of strong fog) and on September 25-26 , Julian days 268-269 (QNX part of disk was full).

b) The retrieval of air-water temperature difference was performed for two averaging times 12 min and 36 sec. The results are in good agreement with in situ measurements. It was also noted that measurements of down welling radiation (brightness temperature above horizon) predict the same sign of stability as analysis based on up welling radiation (sea surface brightness temperature).

c) It can be noted that the variability of air-water temperature difference increases during stable atmospheric conditions.

4. DISCUSSION OF FUTURE DATA ANALYSIS

Additional analysis of COPE 5-mm radiometric data will include the the recovery of air temperature profiles (at minimum estimation of air temperature gradient close to the sea surface) and a more careful study of time variations observed in air-water temperature difference. We consider as very important the comparison of 5-mm radiometric results with wind and fluxes data of C. Fairall, and infrared measurements carried out by APL/UW (A. Jessup). We hope that our data may be useful for interpretation of radar, scatterometric, or other measurements collected during COPE. For example the comparison of radiometric measurements from a blimp with model predictions will be based on 5- mm skin temperatures. Of course we hope that other COPE participants will find opportunities that are unknown to us; all suggestions of joint data analysis are welcome.

Acknowledgments. The work reported in this Memorandum was partially supported by the Advanced Systems Applications Program of the U. S. Department of Defense.

REFERENCES

Trokhimovski, Yu. G. , E. R. Westwater, and Y. Han, 1995a. Air and sea surface temperature measurements using a 60 GHz microwave rotating radiometer. Proceedings, IGARSS'95, Florence, Italy, July 1995, 1110-1112.

Trokhimovski, Yu. and V. Leuskiy, 1993. Measurements of water surface temperature using 5-mm radiometer. Proceedings, IGARSS'93, Tokyo, Japan, August 1993, 1625-1626.

Trokhimovski, Yu. G. , E. R. Westwater, Y. Han, and V. Leuskiy, 1995b. The results of air and sea surface temperature measurements using a 60 GHz microwave rotating radiometer. submitted to IEEE Trans. Geosci. Remote Sensing.

Westwater, E.R. , J. B. Snider, and A.V. Carlson, 1975. Experimental determination of temperature profiles by ground-based microwave radiometry. J. Appl. Meteorol. 14 (4): 524-539.

Westwater, E. R. , 1993. Ground-based Microwave Remote Sensing of Meteorological Variables. In Atmospheric Remote Sensing by Microwave Radiometry. M. A. Janssen, (Ed.), J. Wiley & Sons, Inc., New York, 145-213.

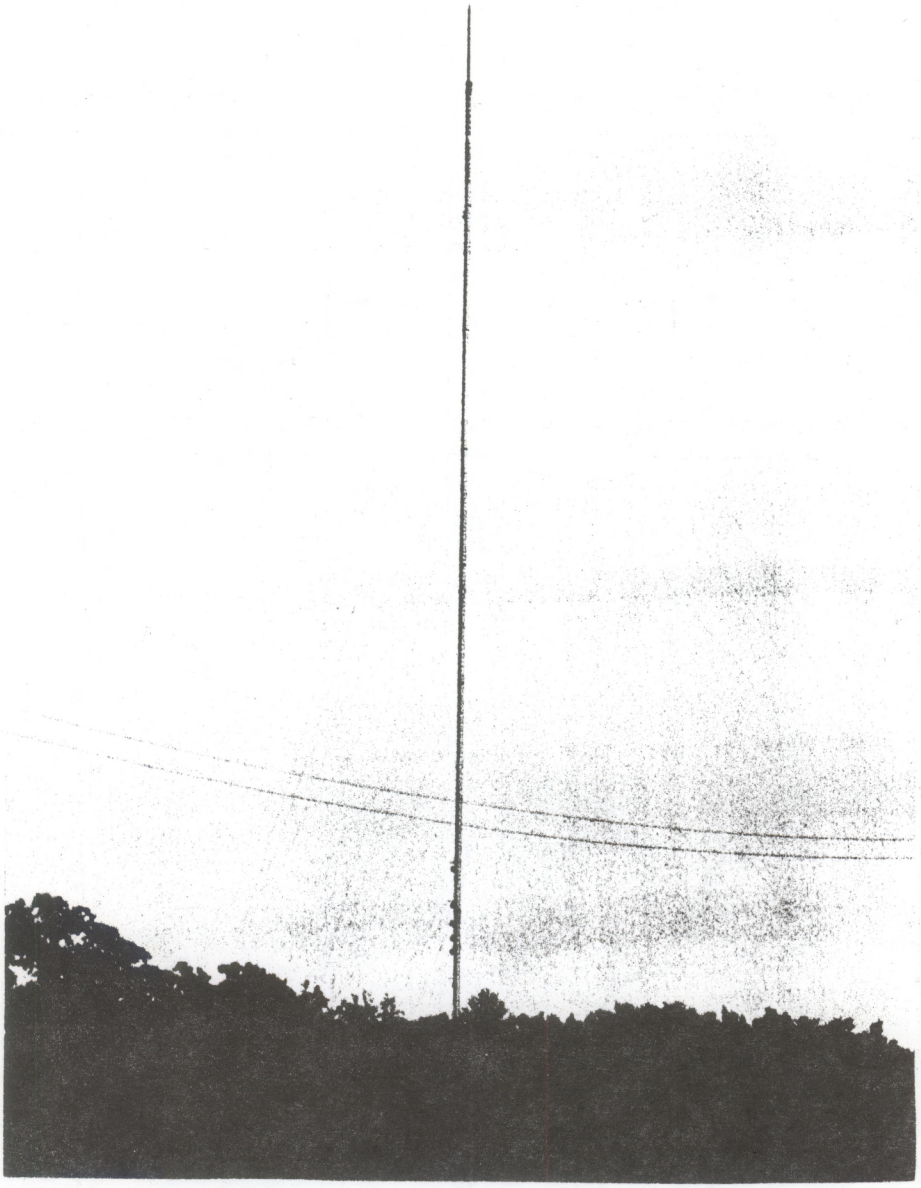

Fig. 1. Photo of the 300 m meteorological tower at the Boulder Atmospheric Observatory.

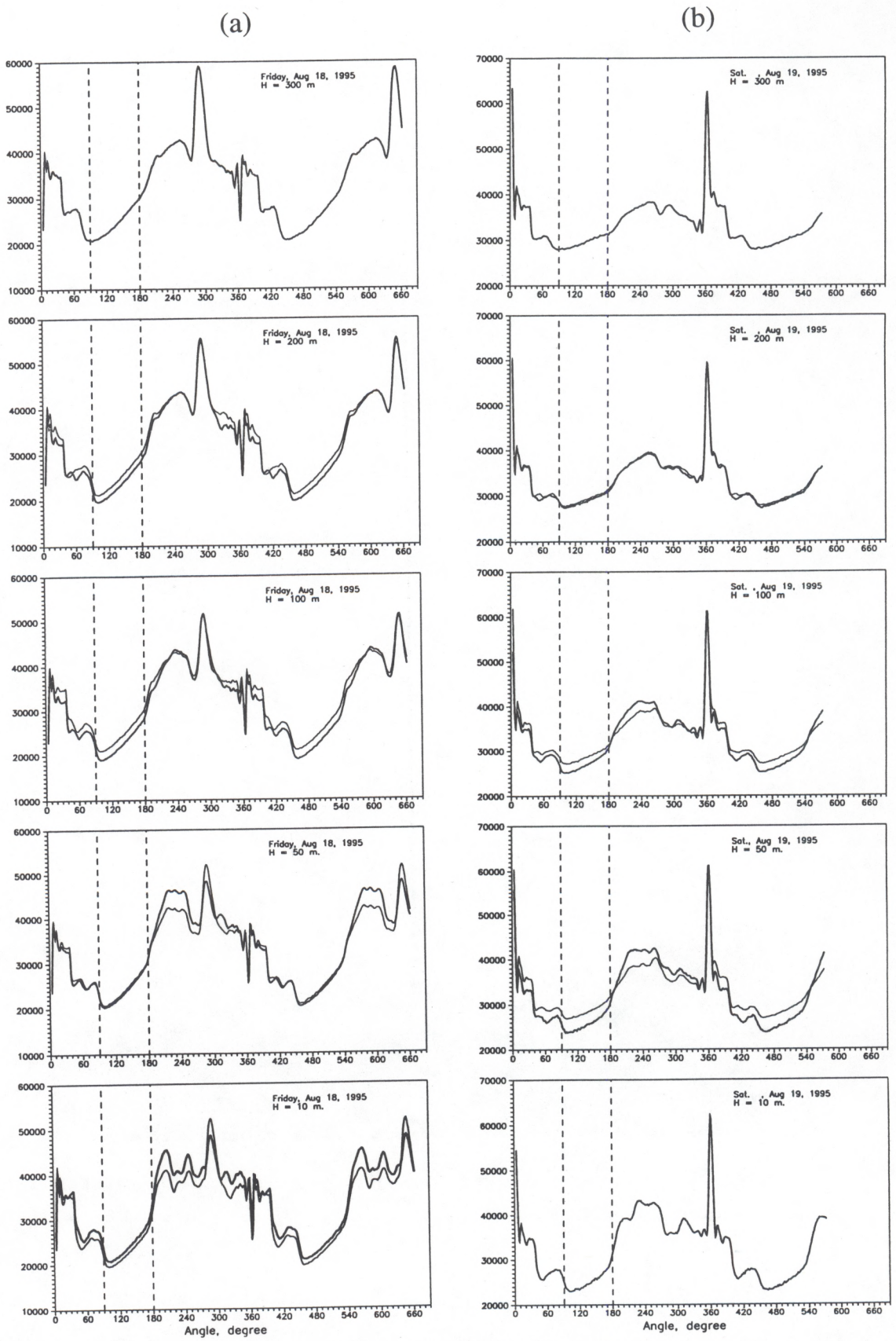

Fig. 2. Two days of radiometric data taken at the BAO. The ordinate shows voltage counts. The angles $0° \leq \theta \leq 90°$ view the tower; the angles $90° \leq \theta \leq 180°$ view the atmosphere; the angles $180° \leq \theta \leq 360°$ view the ground.

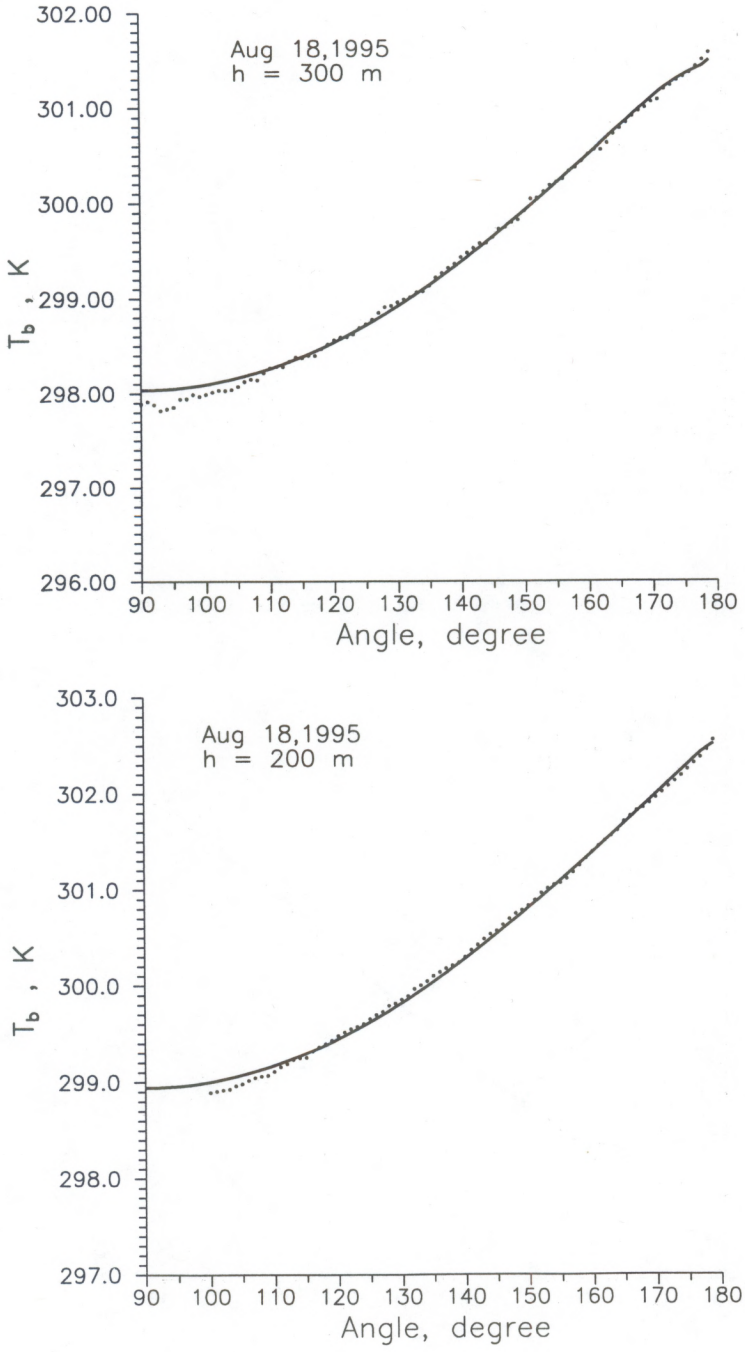

Fig. 3. Comparison of measurements (dotted) and calculations (solid) made at the BAO.

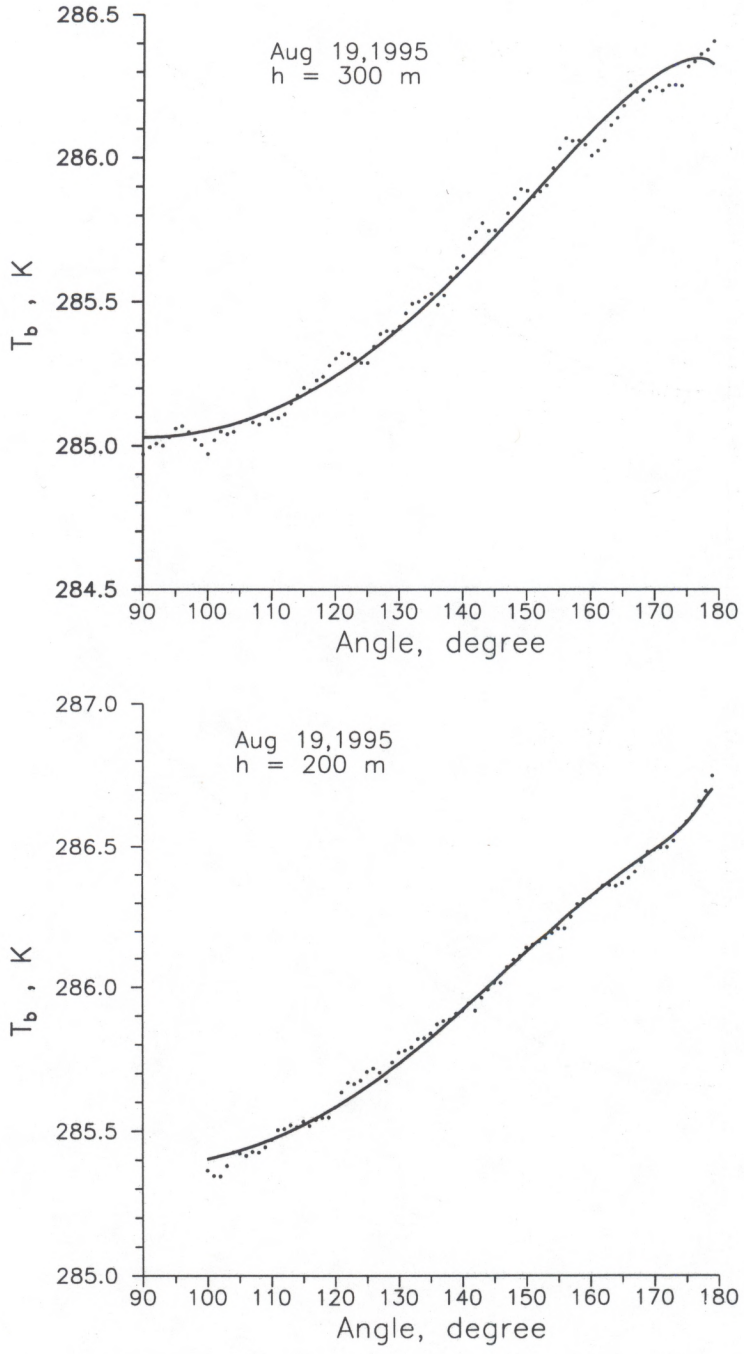

Fig. 4. Comparison of measurements (dotted) and calculations (solid) made at the BAO.

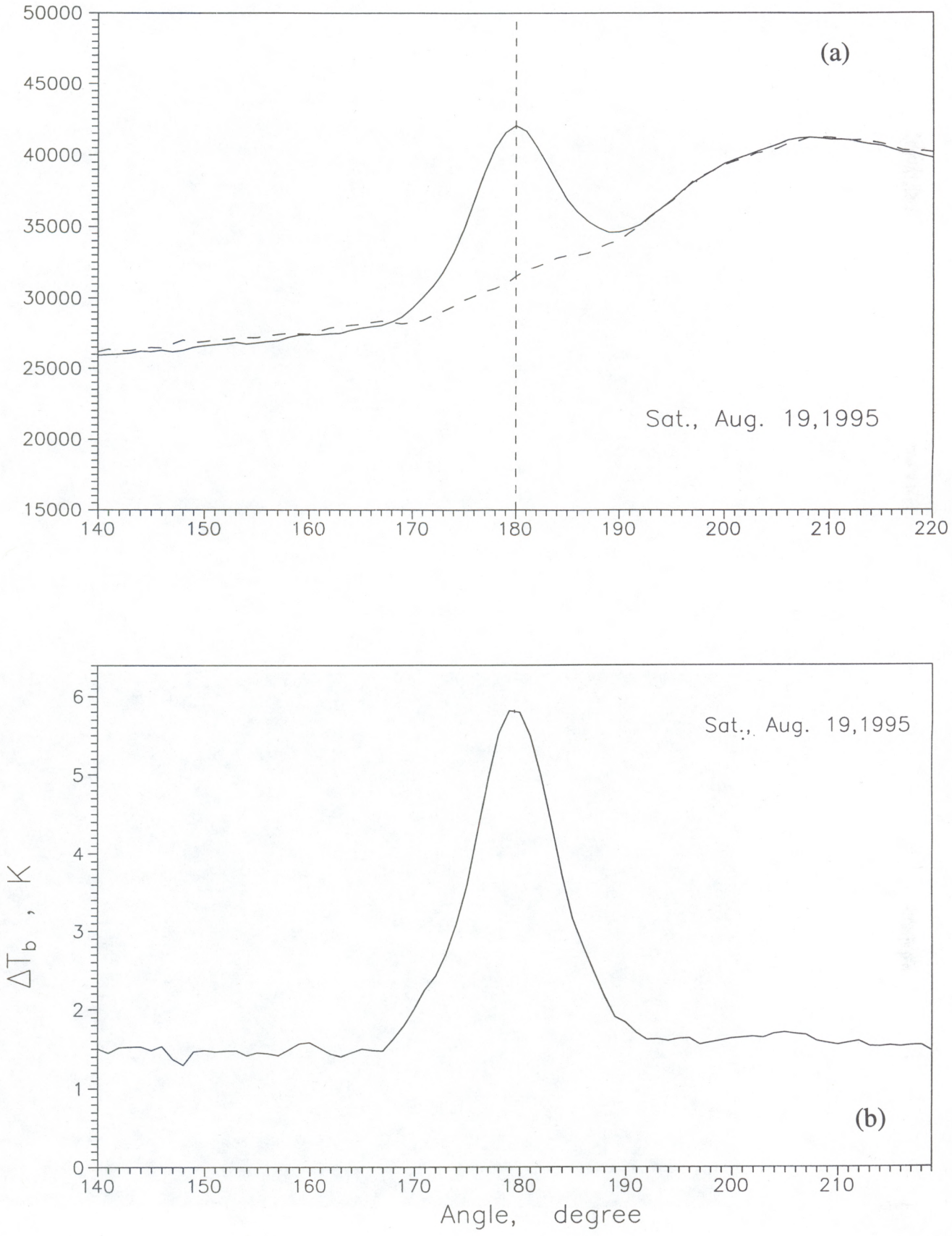

Fig. 5. (a) Measurements of radiometer with flourescent light turned on (top) and off (bottom)
(b) Difference of two curves in (a).

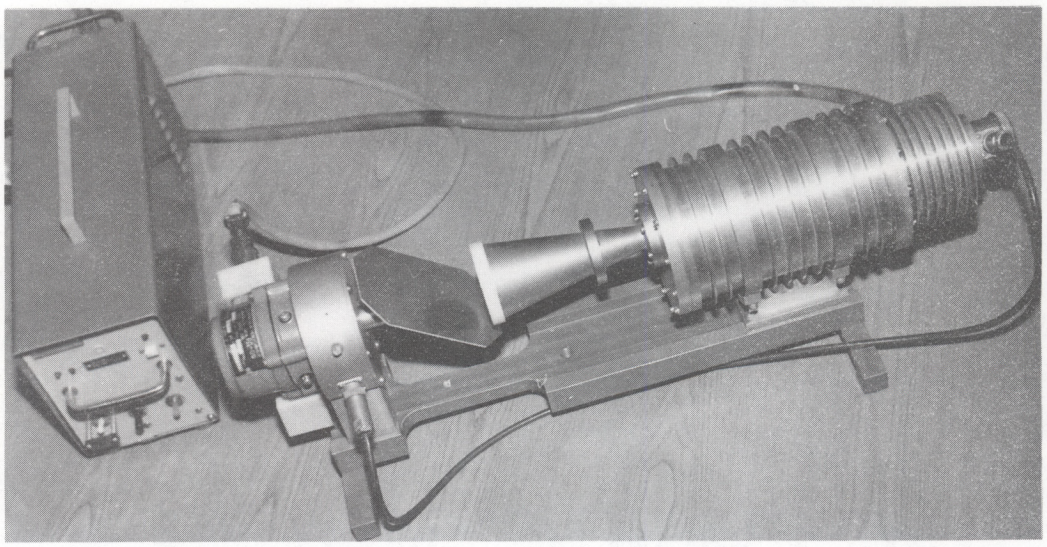

Fig. 6. Photo of 5-mm scanning radiometer.

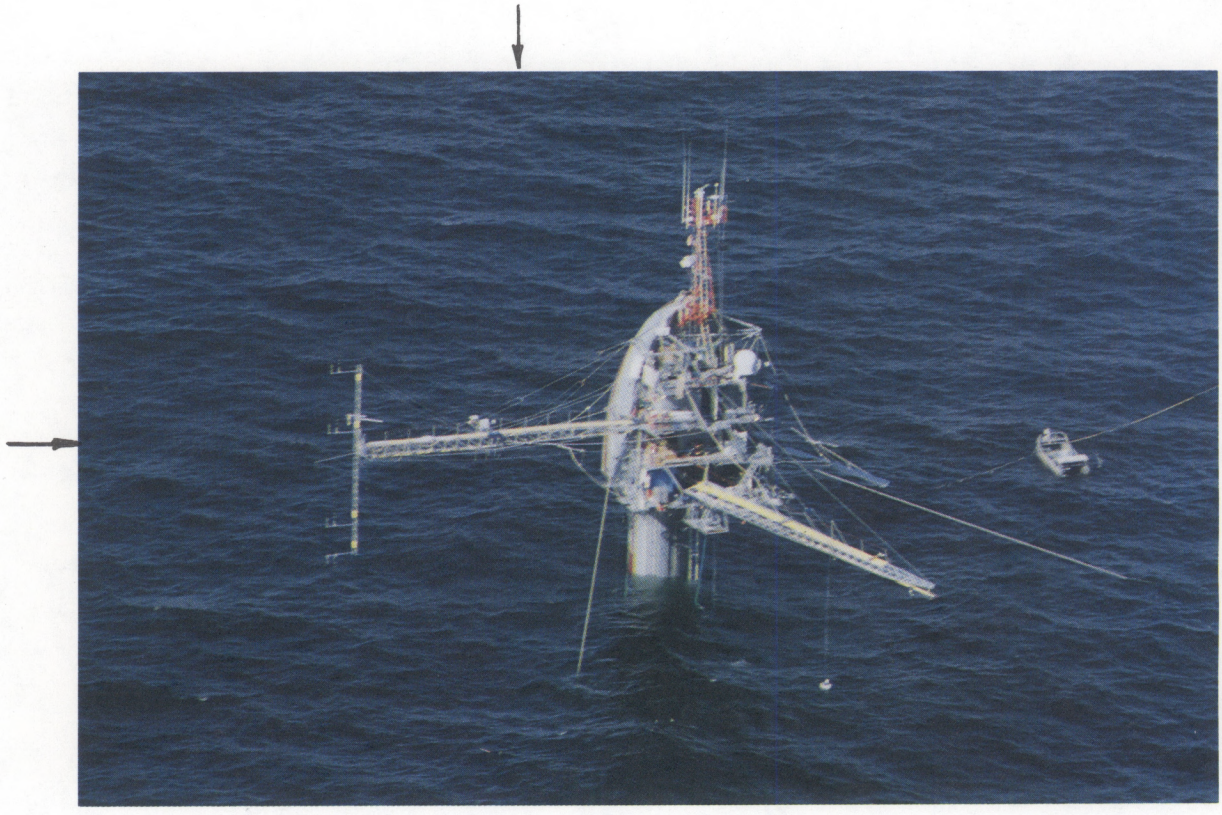

Fig. 7. Photo of FLIP taken from a blimp during COPE. The 5-mm radiometer was installed on the port boom in the left side of the figure.

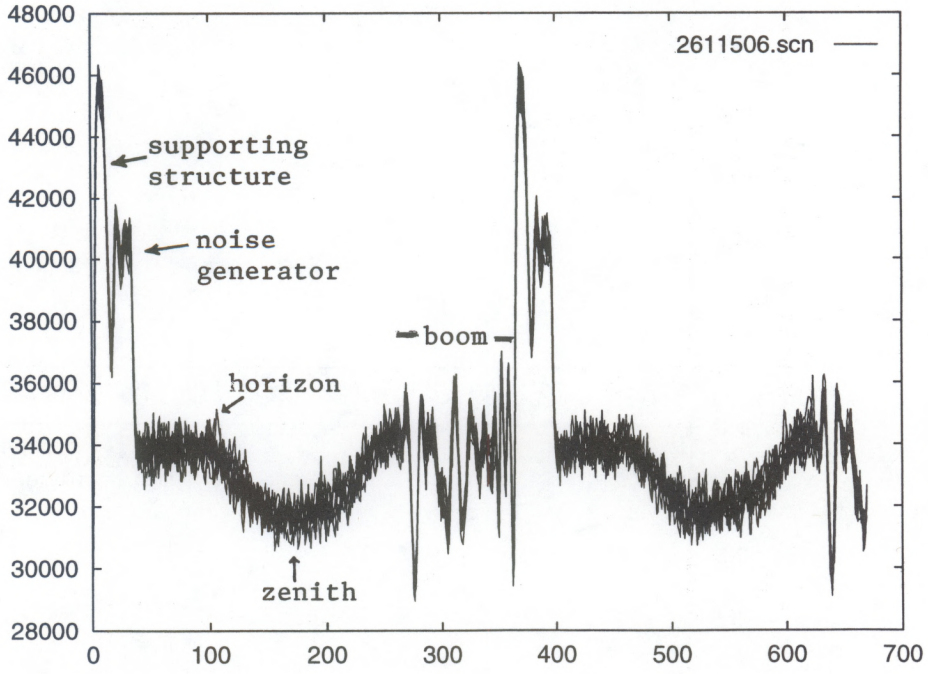

Fig. 8. Example of two scans of raw radiometer data taken on FLIP. Various features observed by the radiometer are indicated.

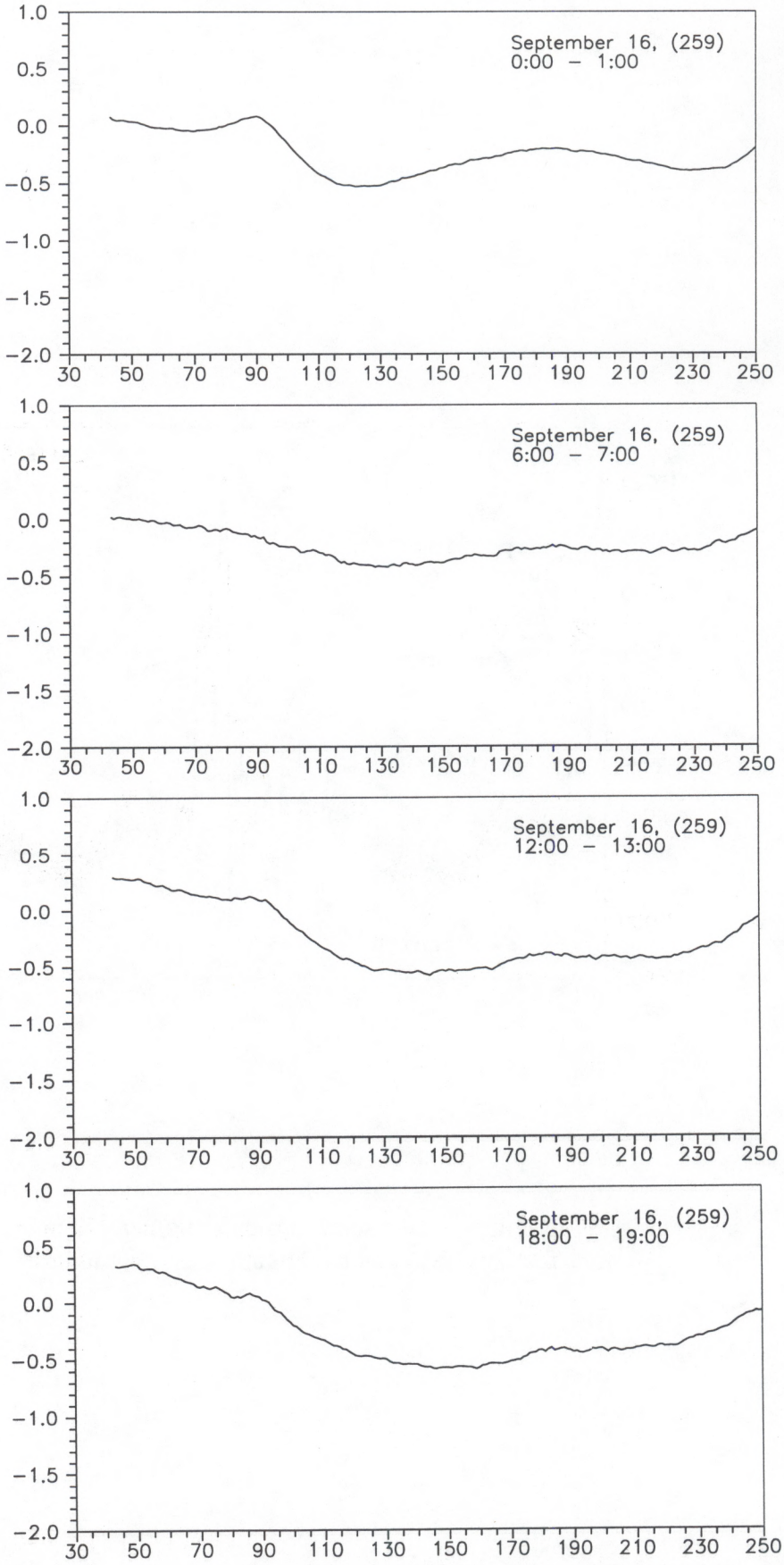

Fig. 9. 1-h averages of radiometer data (K) as a function of angle relative to nadir. A constant offset has been subtracted from the data.

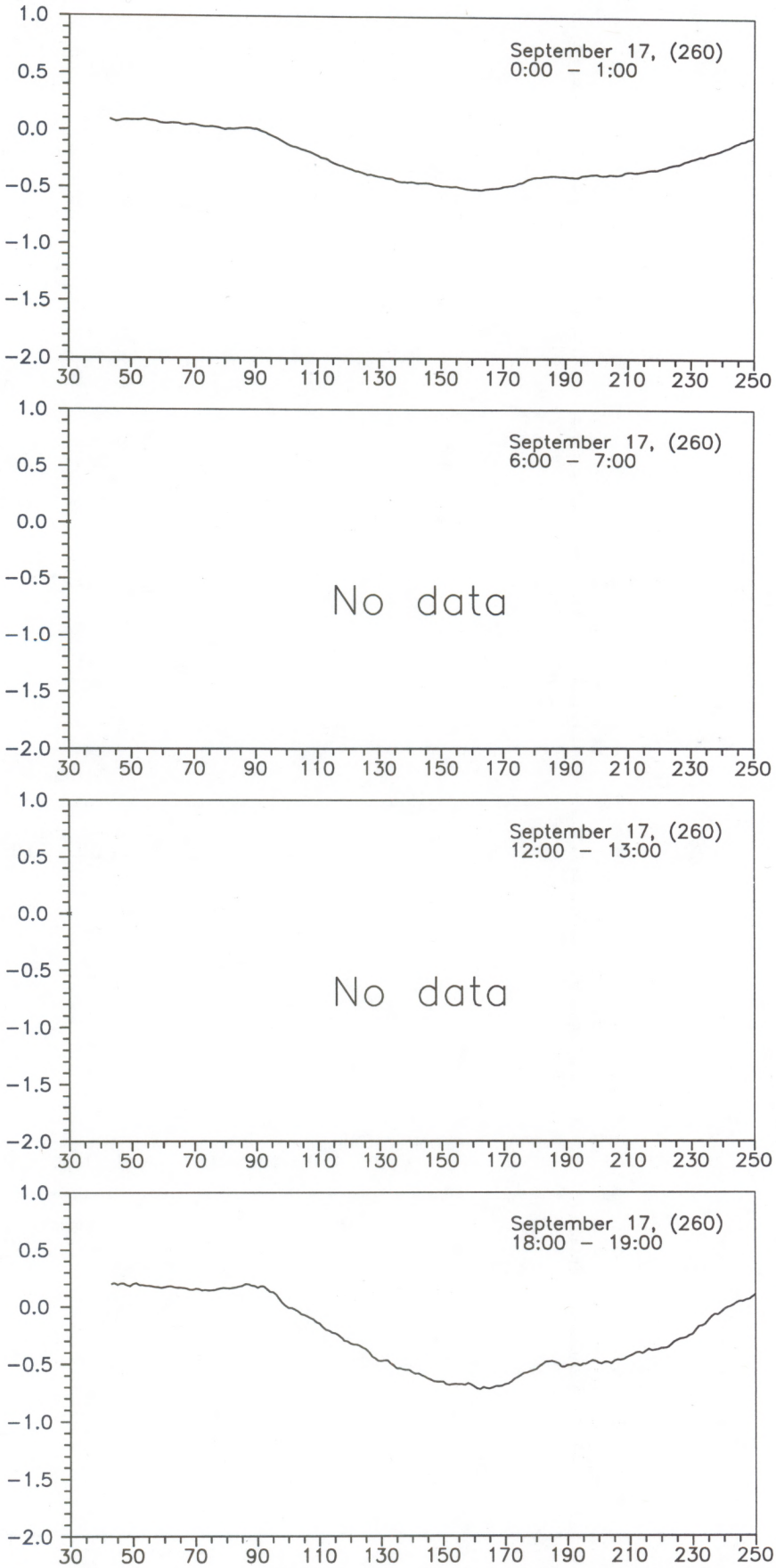

Fig. 10. 1-h averages of radiometer data (K) as a function of angle relative to nadir. A constant offset has been subtracted from the data.

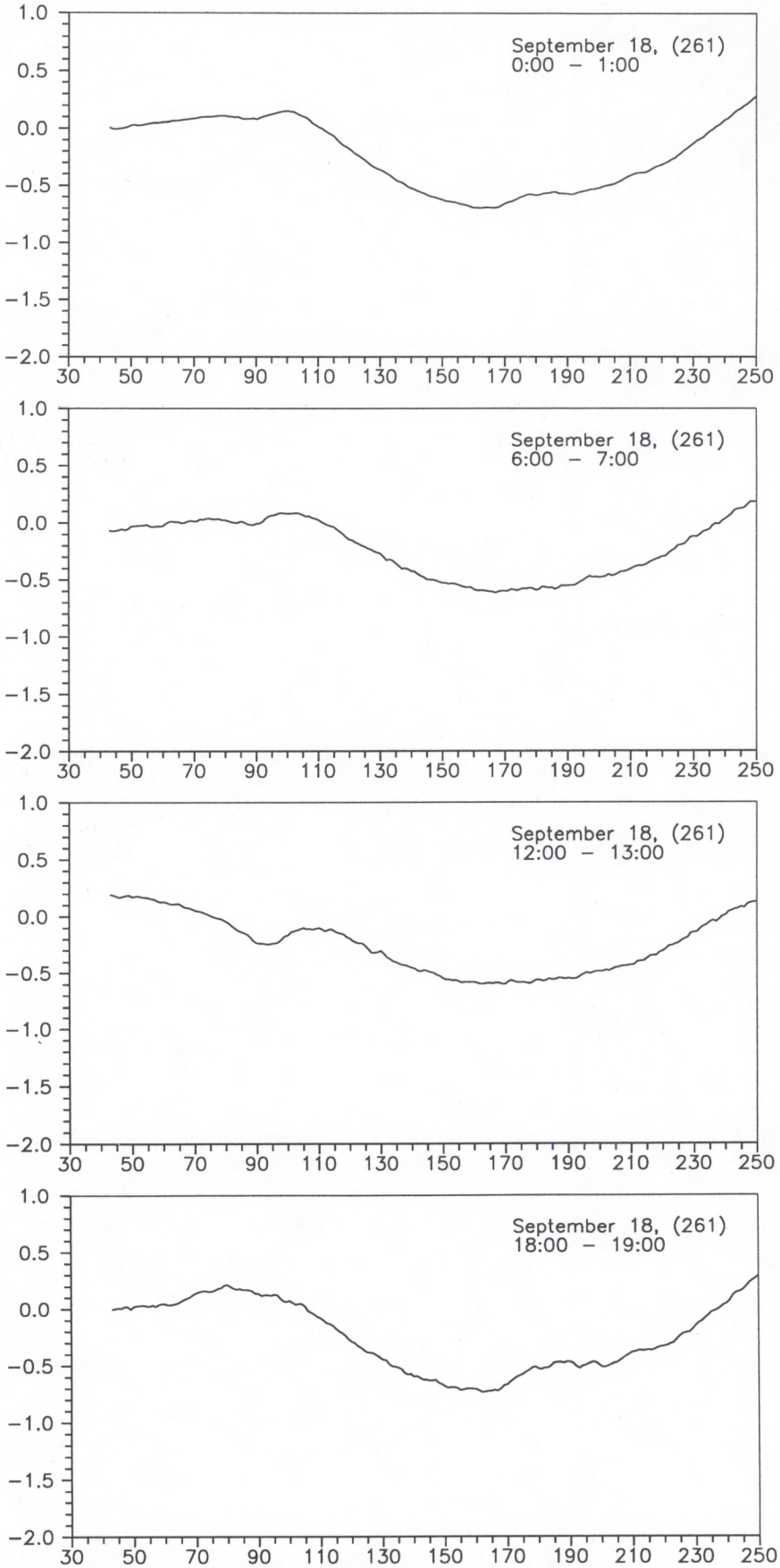

Fig. 11. 1-h averages of radiometer data (K) as a function of angle relative to nadir. A constant offset has been subtracted from the data.

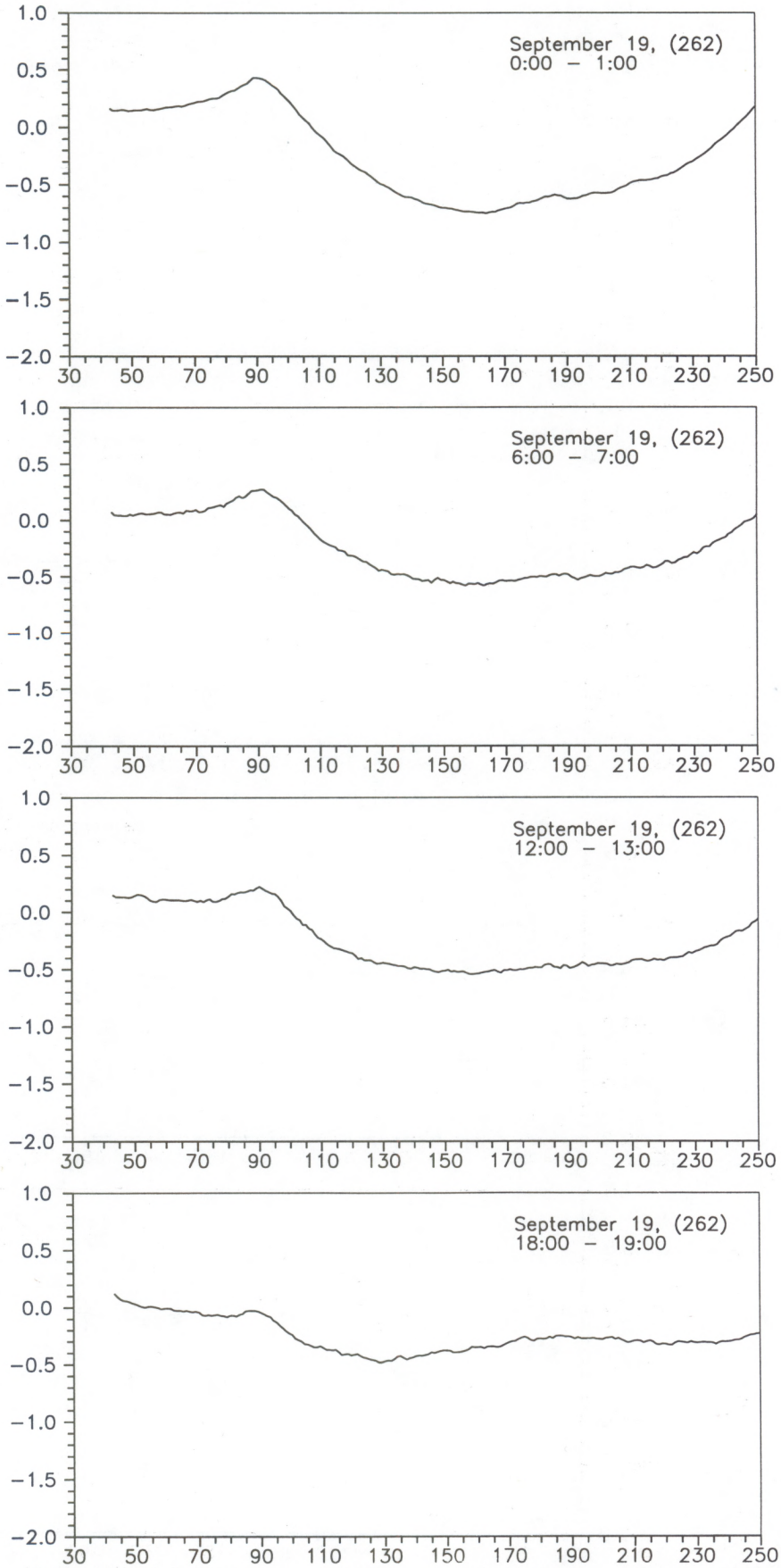

Fig. 12. 1-h averages of radiometer data (K) as a function of angle relative to nadir. A constant offset has been subtracted from the data.

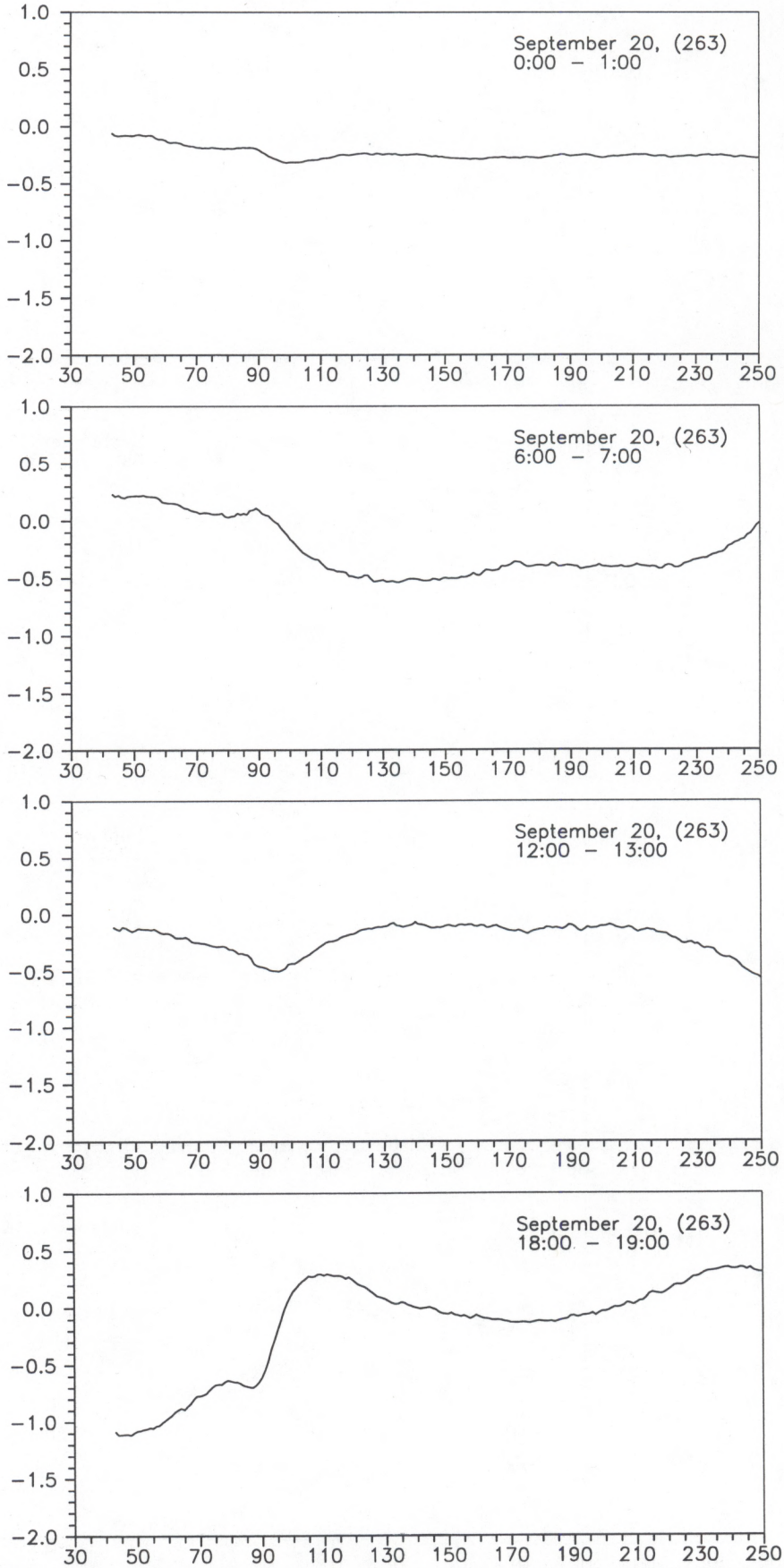

Fig. 13. 1-h averages of radiometer data (K) as a function of angle relative to nadir. A constant offset has been subtracted from the data.

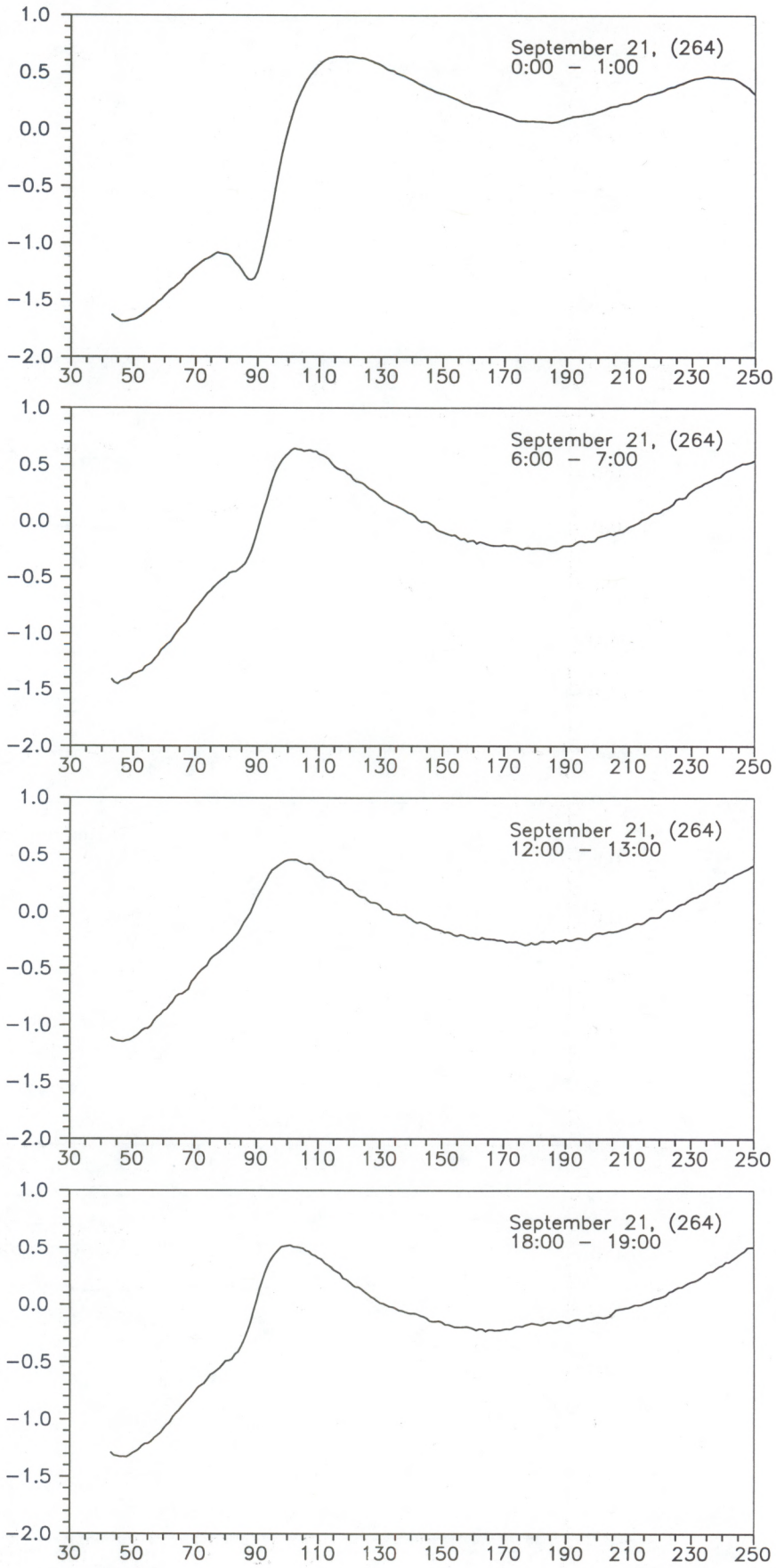

Fig. 14. 1-h averages of radiometer data (K) as a function of angle relative to nadir. A constant offset has been subtracted from the data.

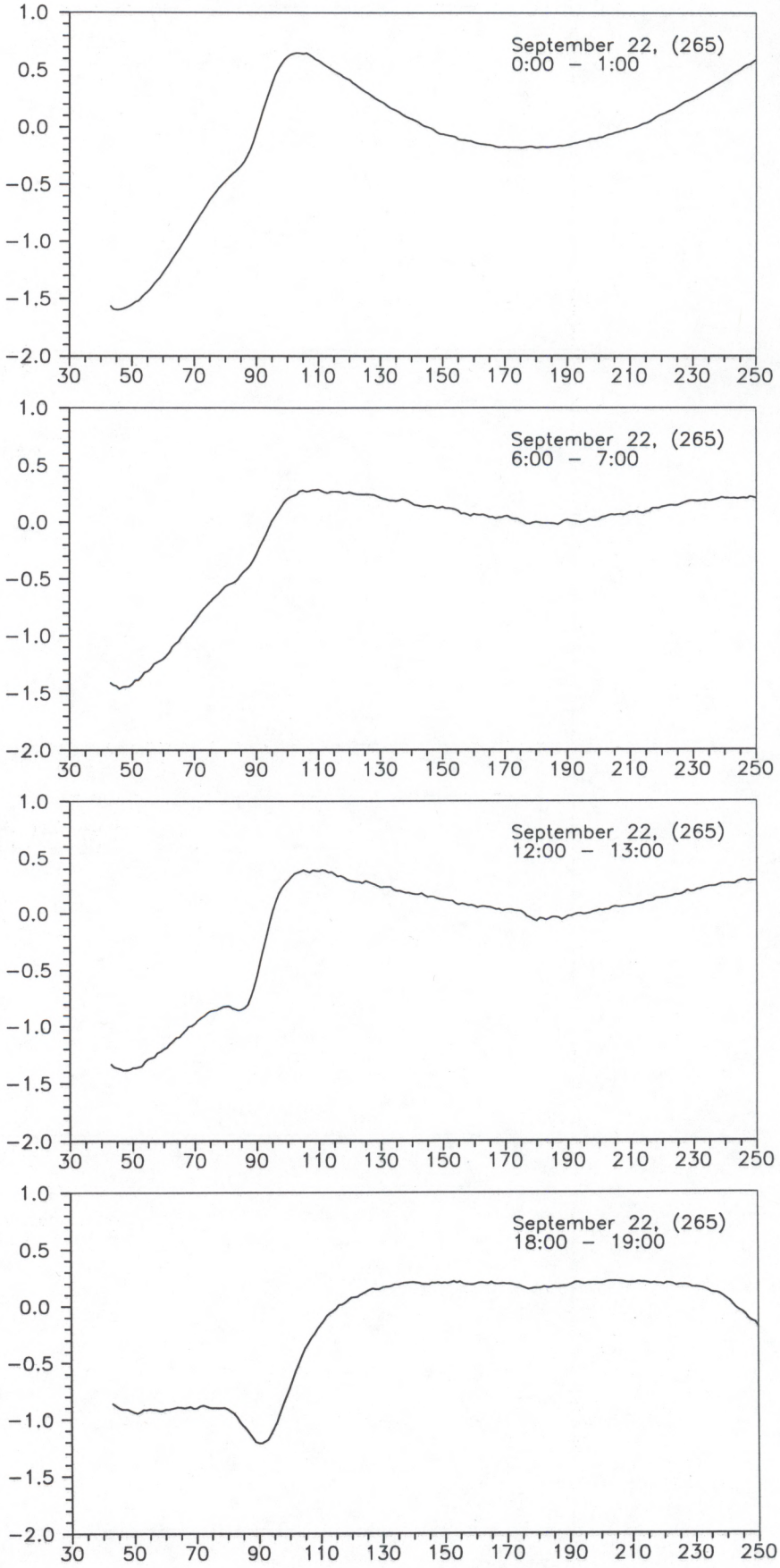

Fig. 15. 1-h averages of radiometer data (K) as a function of angle relative to nadir. A constant offset has been subtracted from the data.

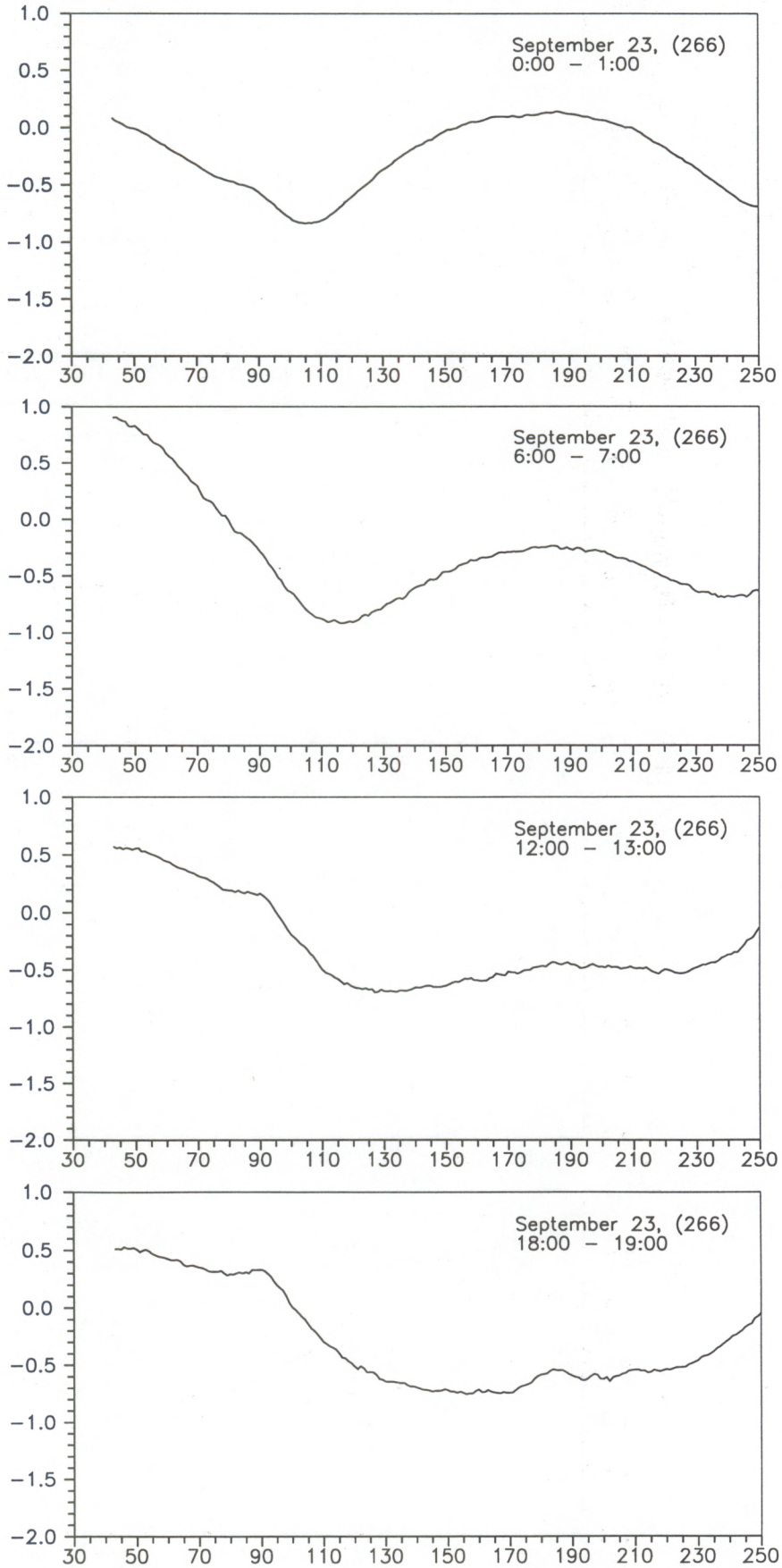

Fig. 16. 1-h averages of radiometer data (K) as a function of angle relative to nadir. A constant offset has been subtracted from the data.

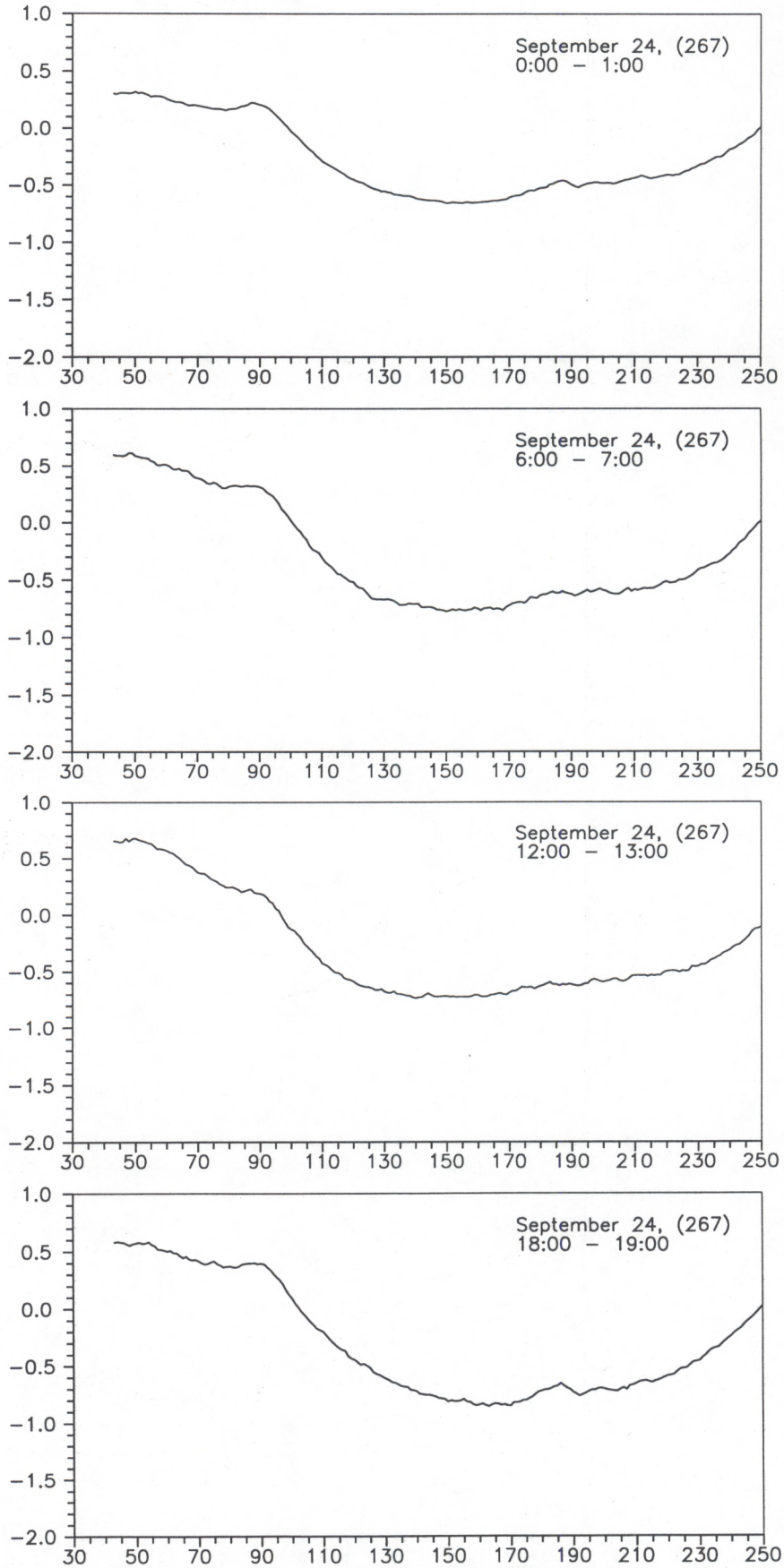

Fig. 17. 1-h averages of radiometer data (K) as a function of angle relative to nadir. A constant offset has been subtracted from the data.

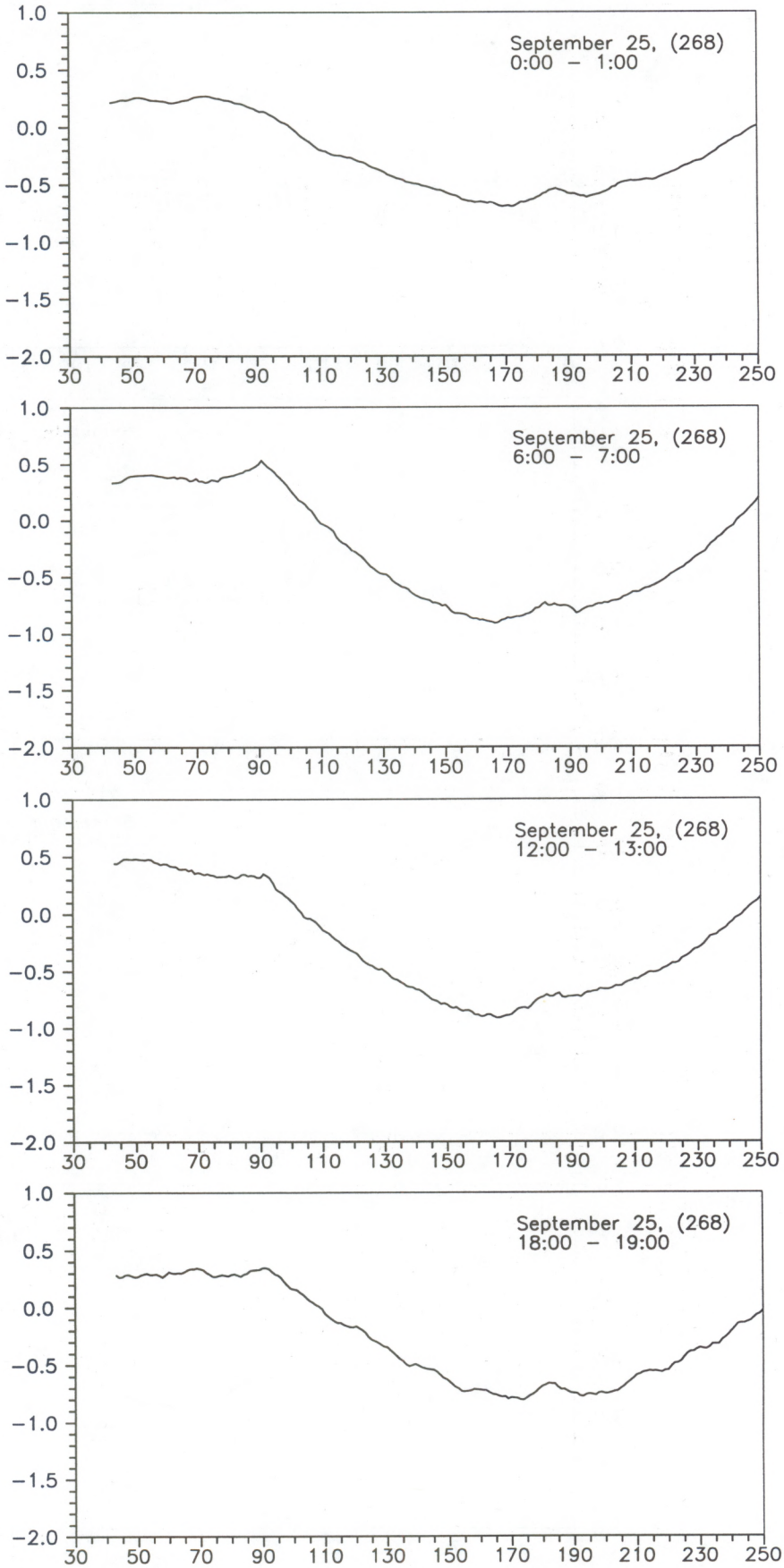

Fig. 18. 1-h averages of radiometer data (K) as a function of angle relative to nadir. A constant offset has been subtracted from the data.

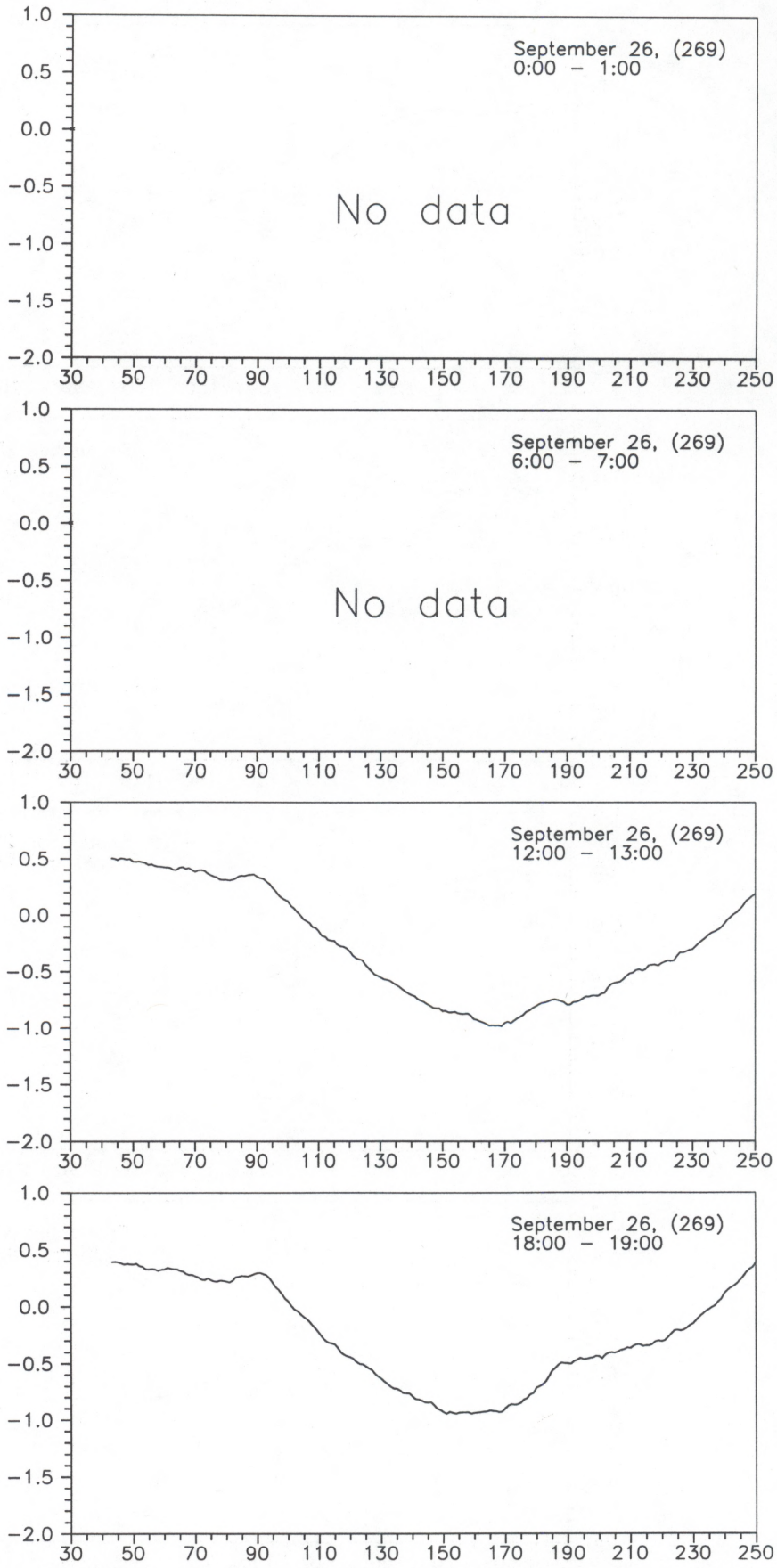

Fig. 19. 1-h averages of radiometer data (K) as a function of angle relative to nadir. A constant offset has been subtracted from the data.

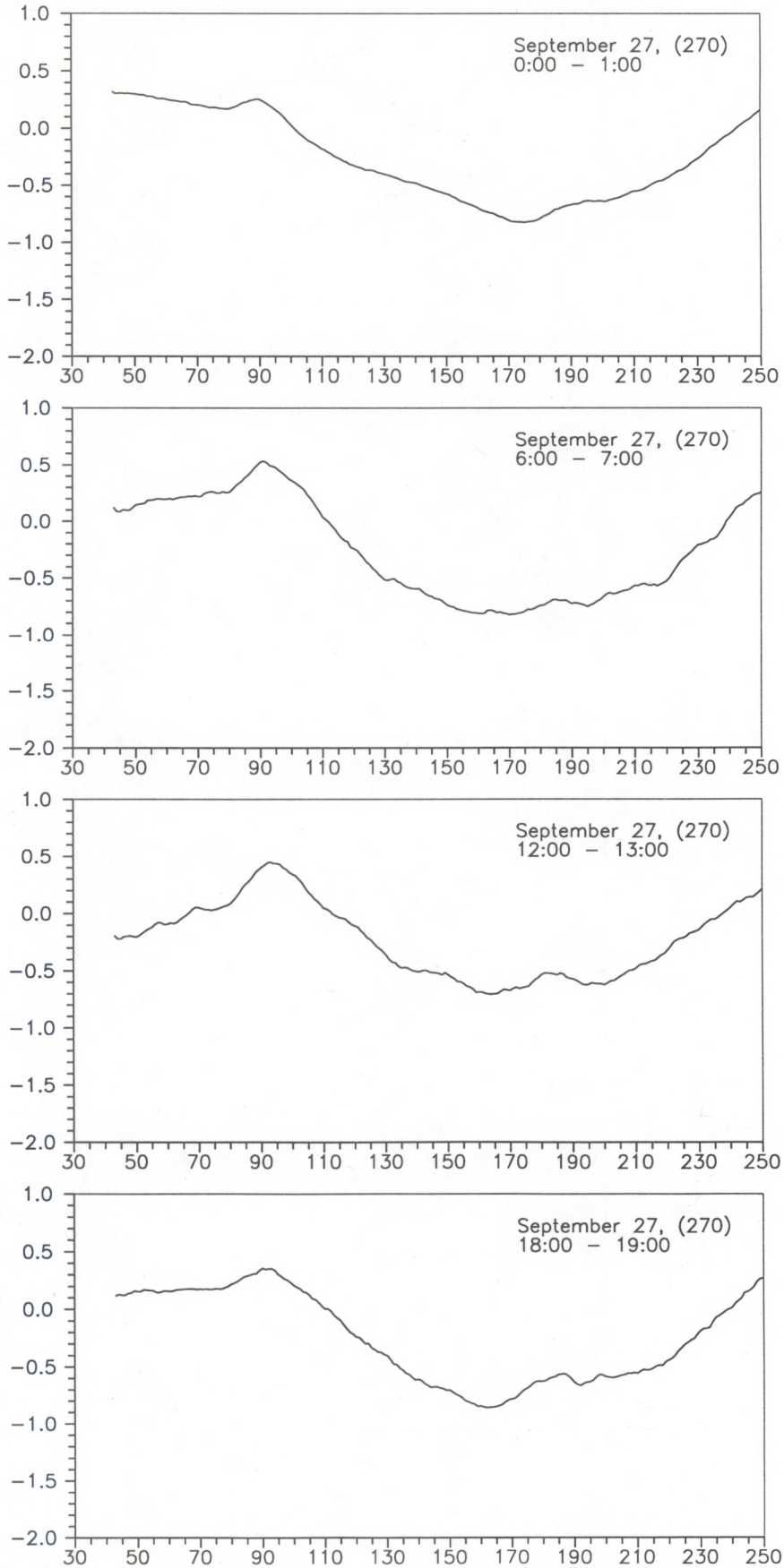

Fig. 20. 1-h averages of radiometer data (K) as a function of angle relative to nadir. A constant offset has been subtracted from the data.

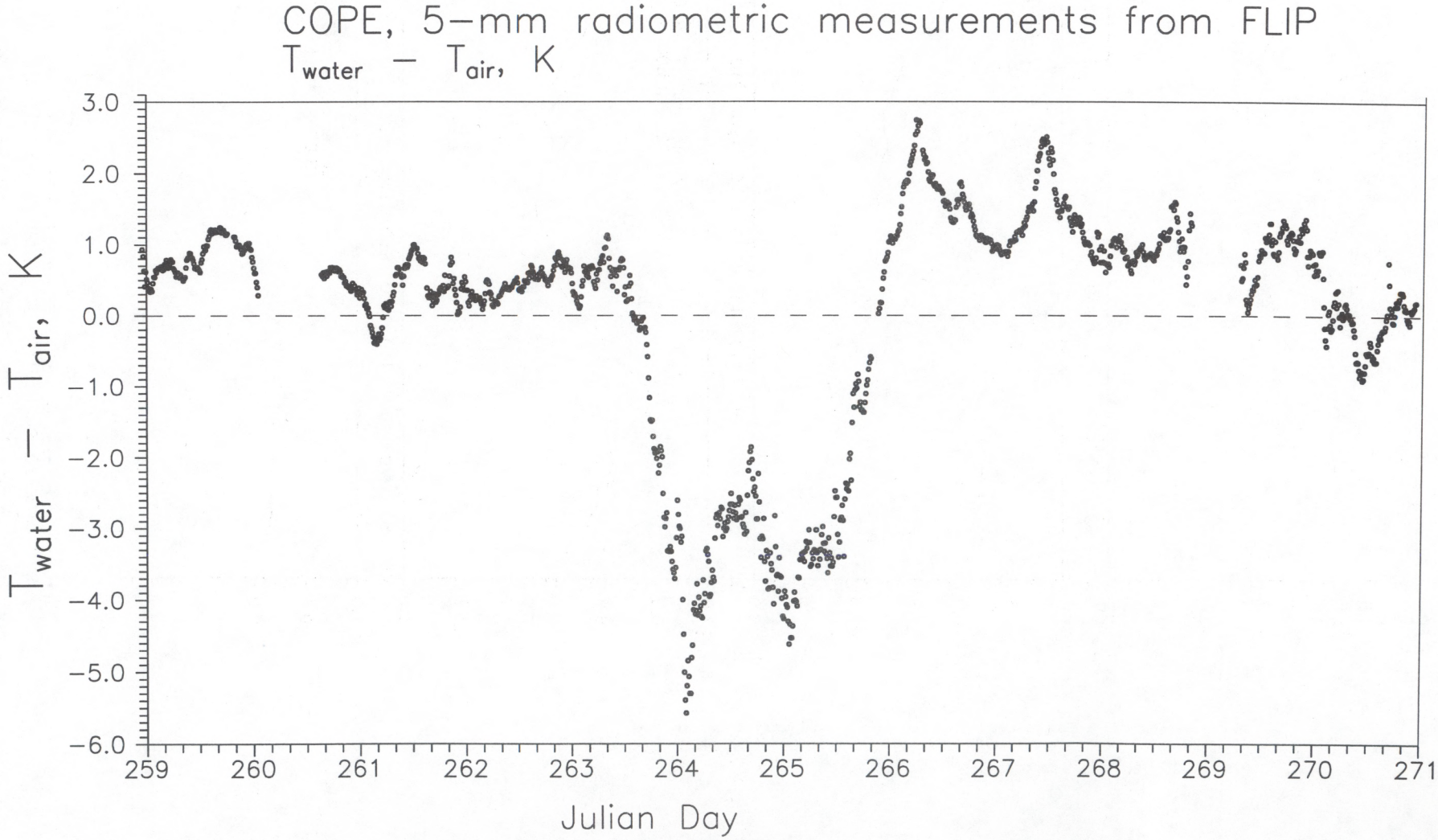

Fig. 21. Time series of sea/air temperature difference taken by the 5-mm radiometer during COPE.

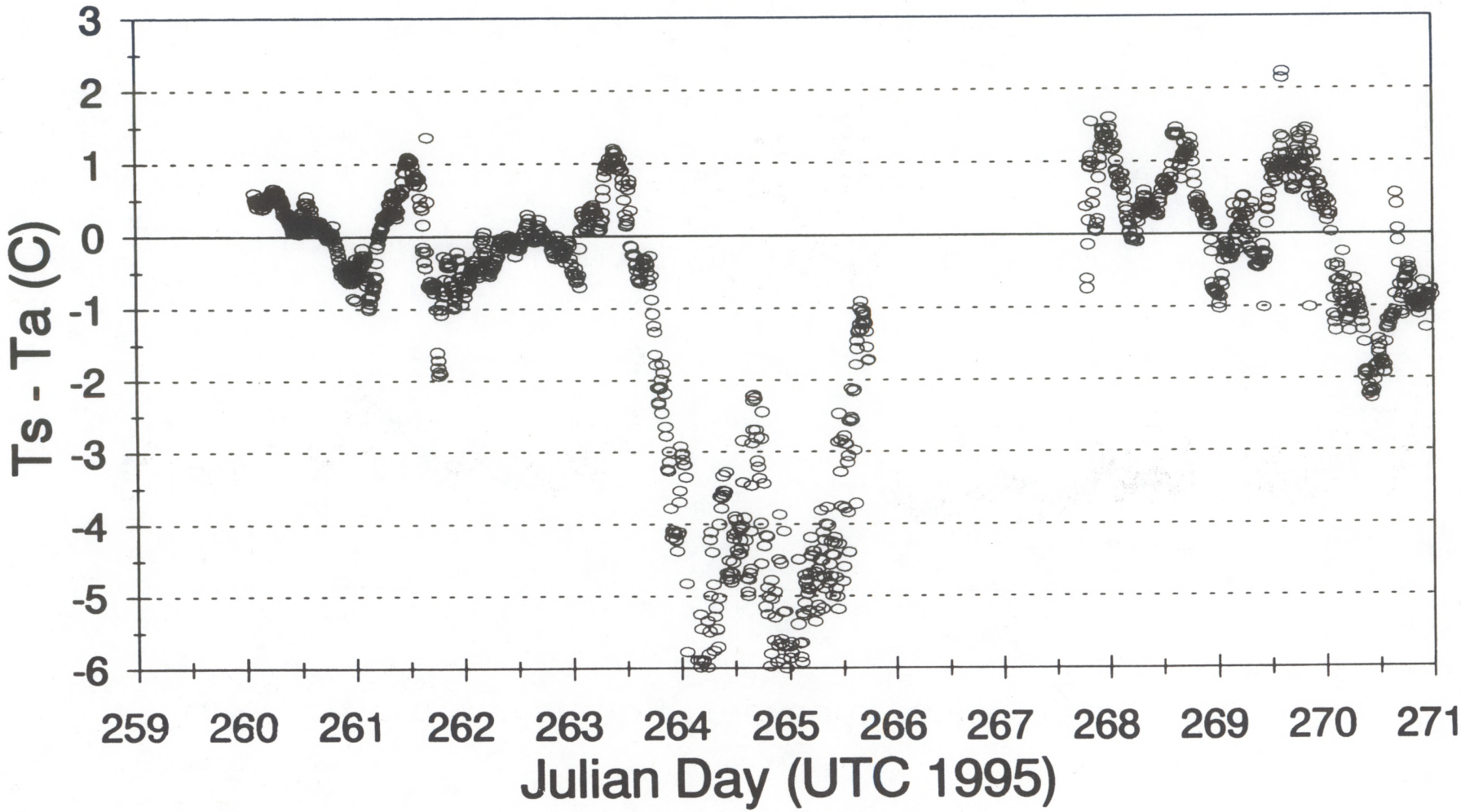

Fig. 22. Time series of sea/air temperature difference taken by in situ instruments during COPE.

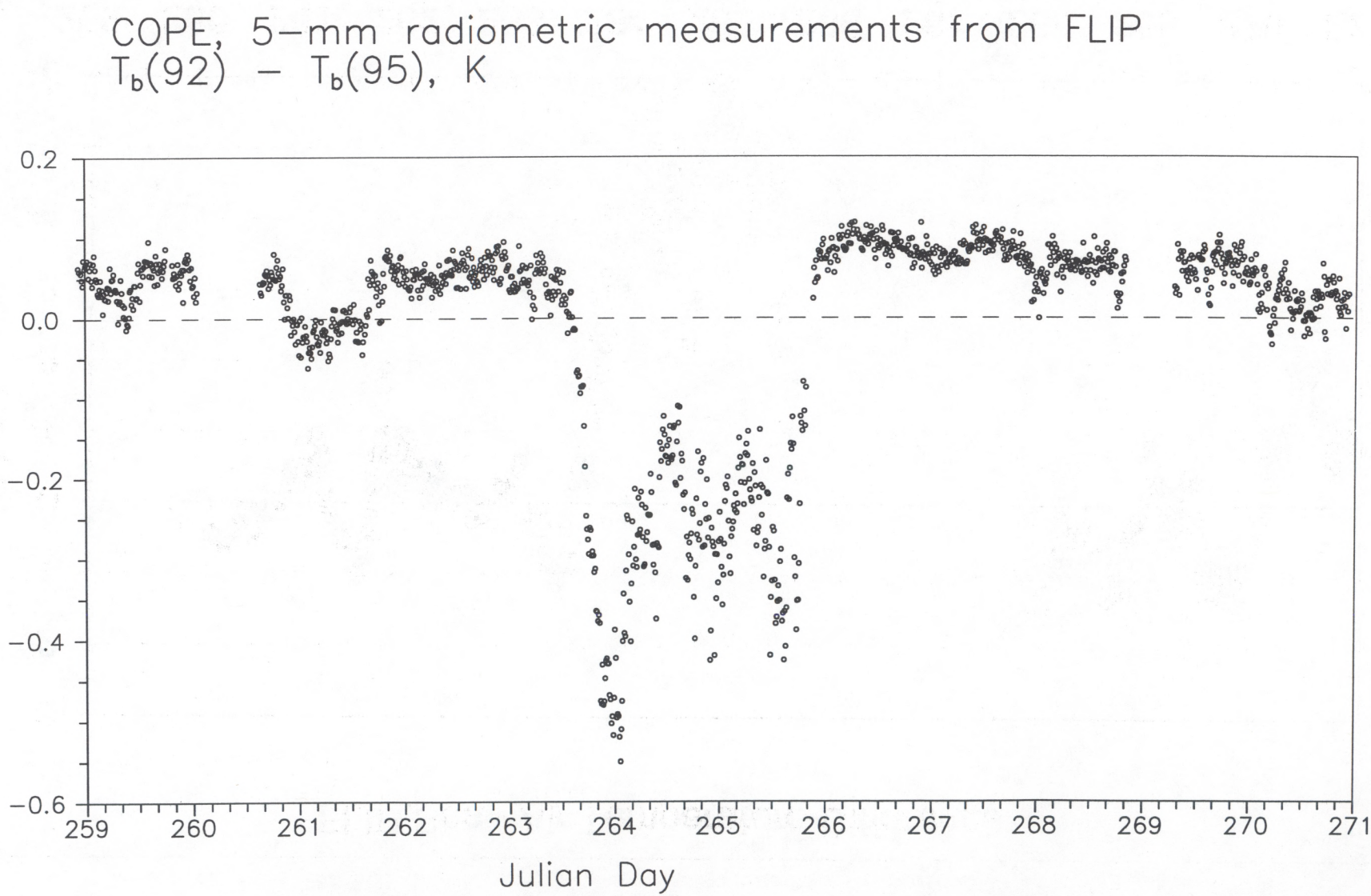

Fig. 23. Time series of the difference of brightness temperatures at nadir angles 92° and 95°.

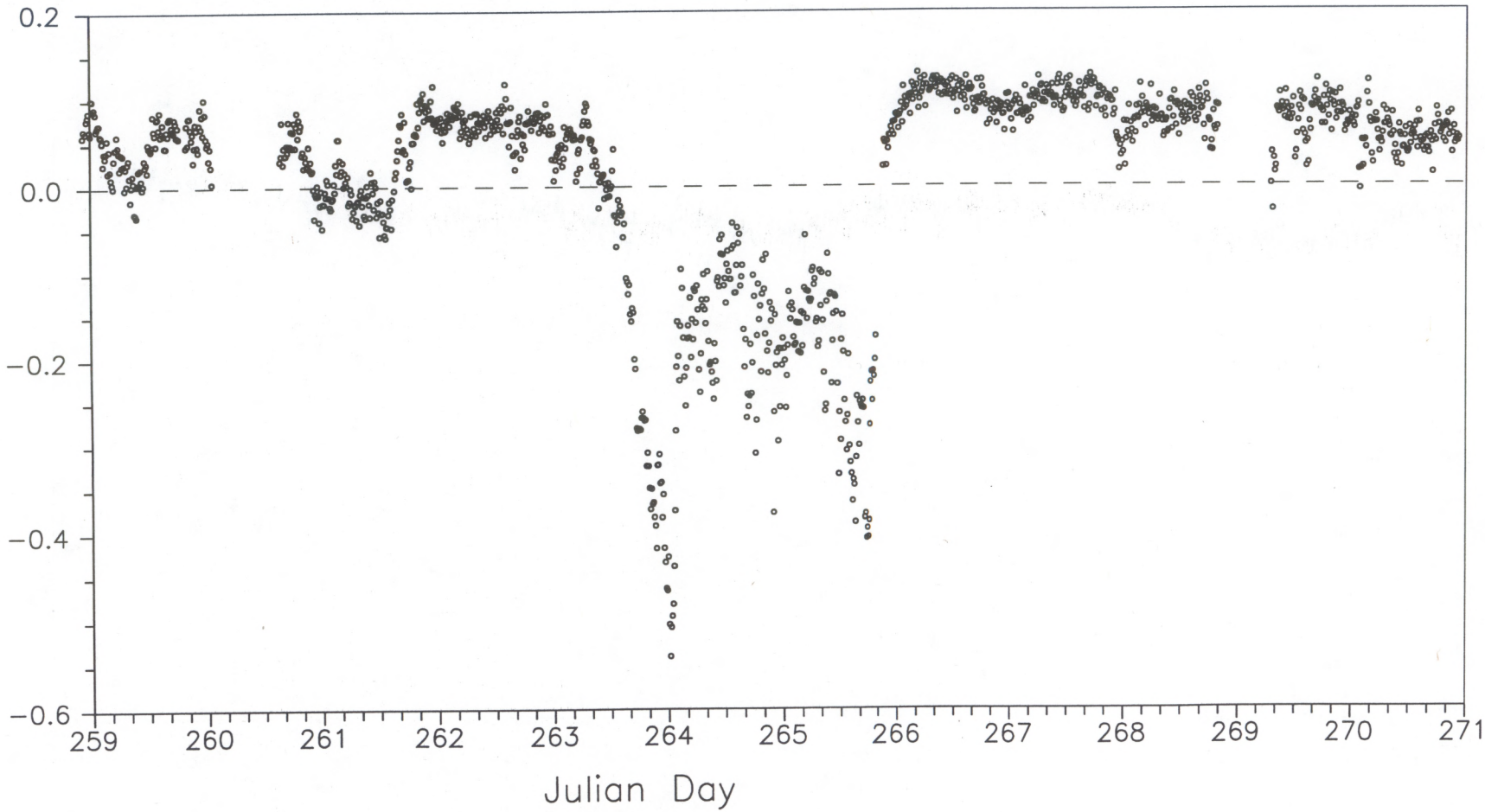

Fig. 24. Time series of the difference of brightness temperatures at nadir angles 95° and 98°.

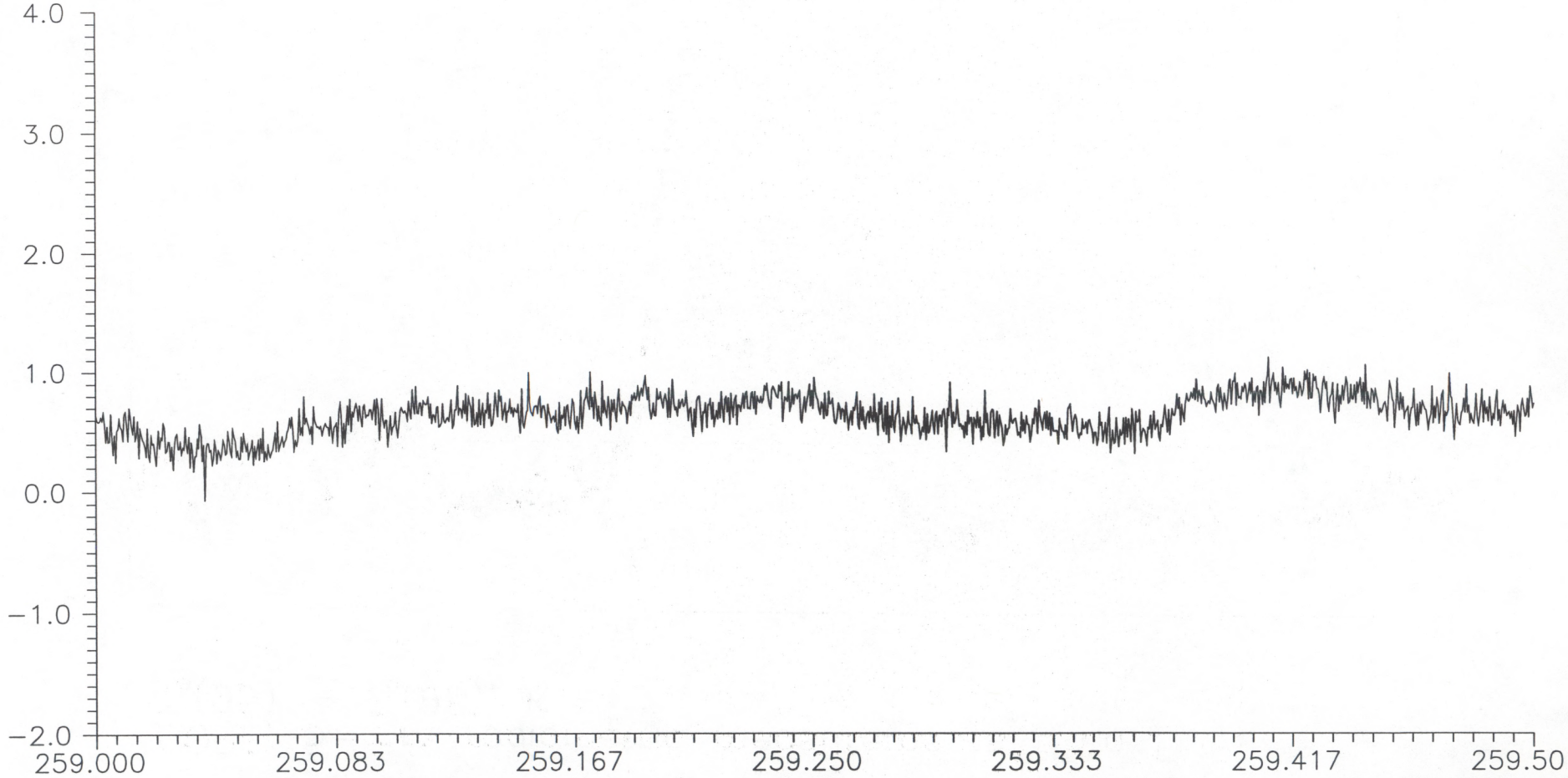

Fig. 25. Time series of 36-s averaged radiometrically-derived sea/air temperature difference.

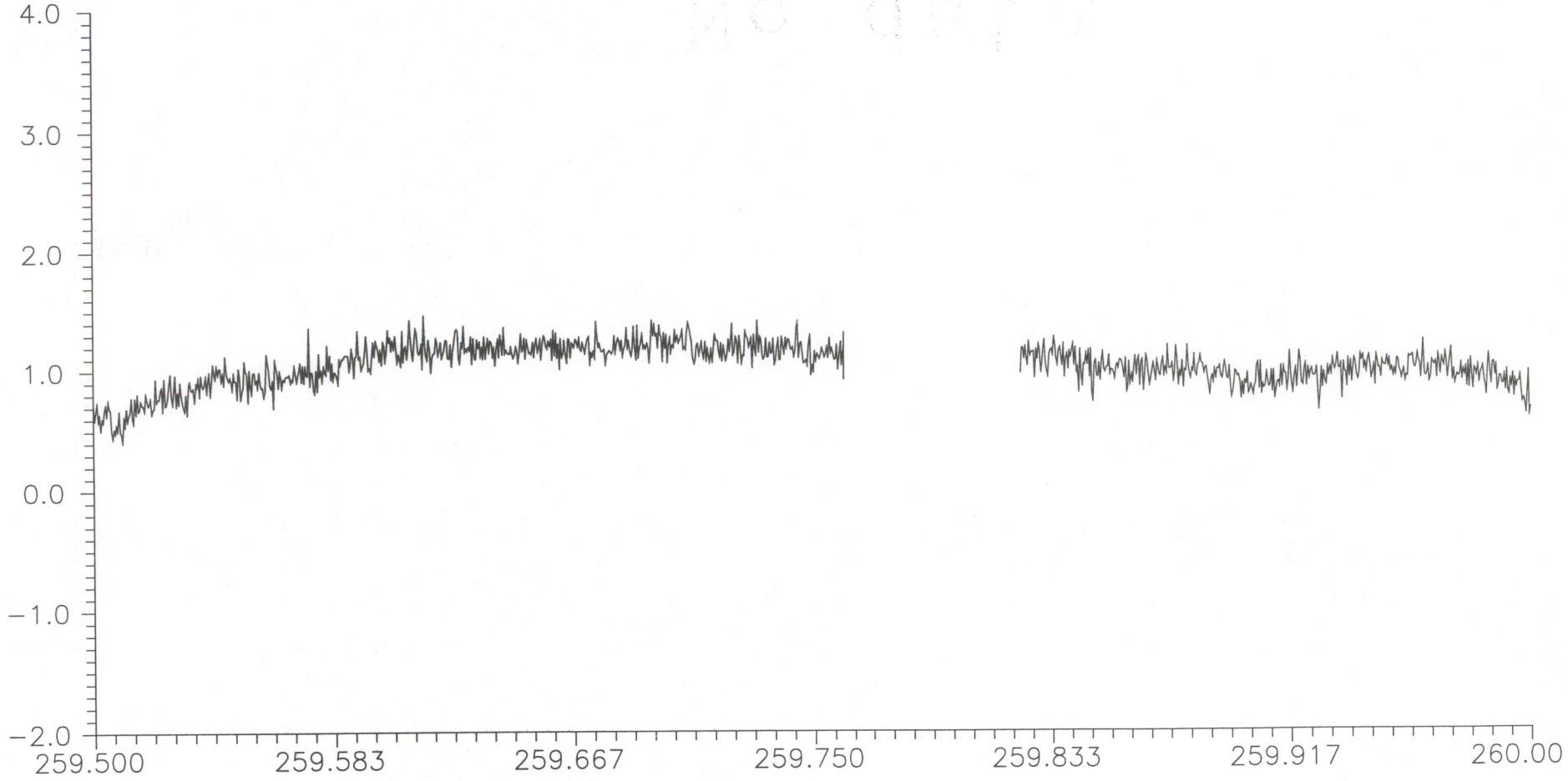

Fig. 26. Time series of 36-s averaged radiometrically-derived sea/air temperature difference.

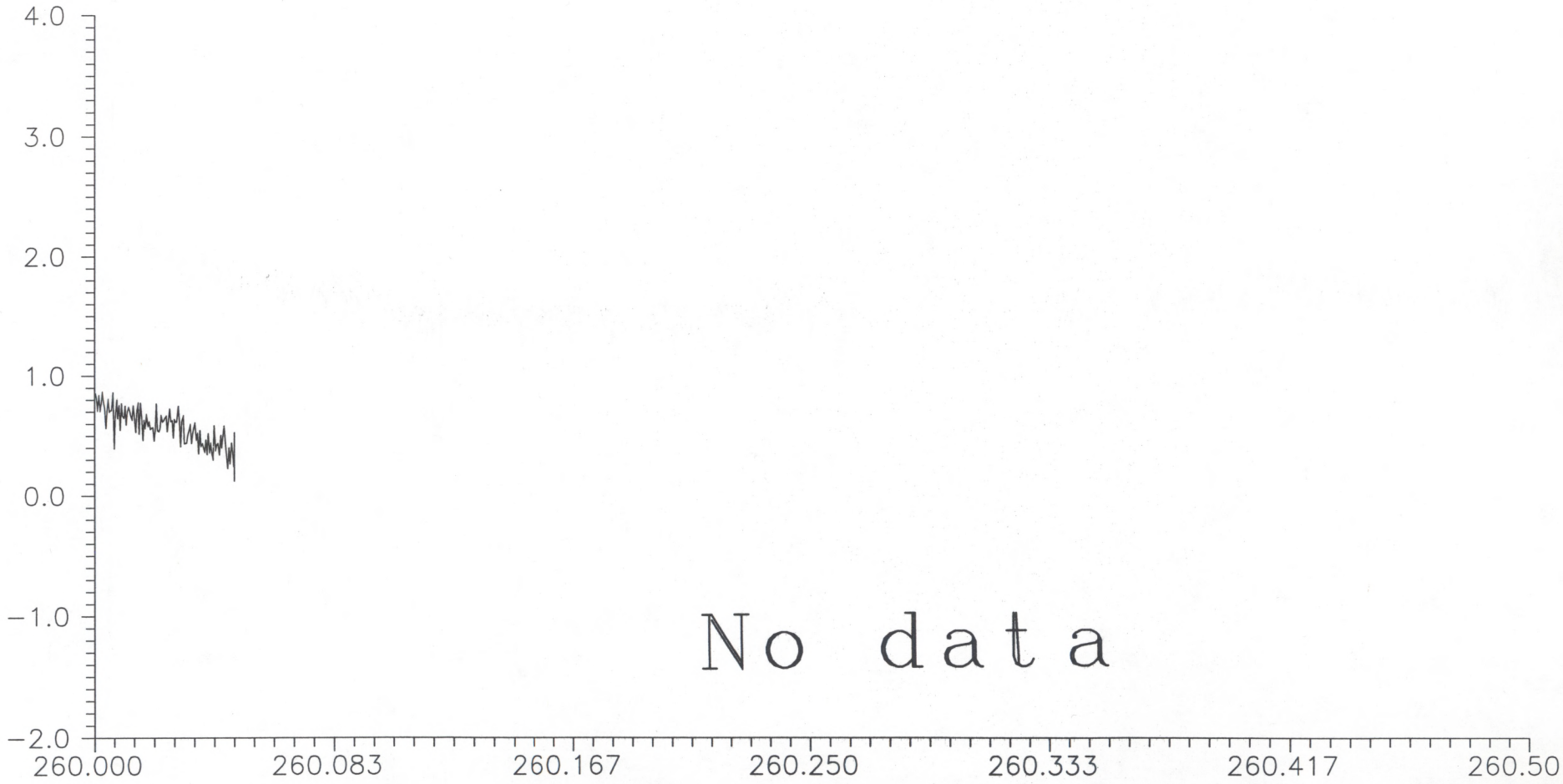

Fig. 27. Time series of 36-s averaged radiometrically-derived sea/air temperature difference.

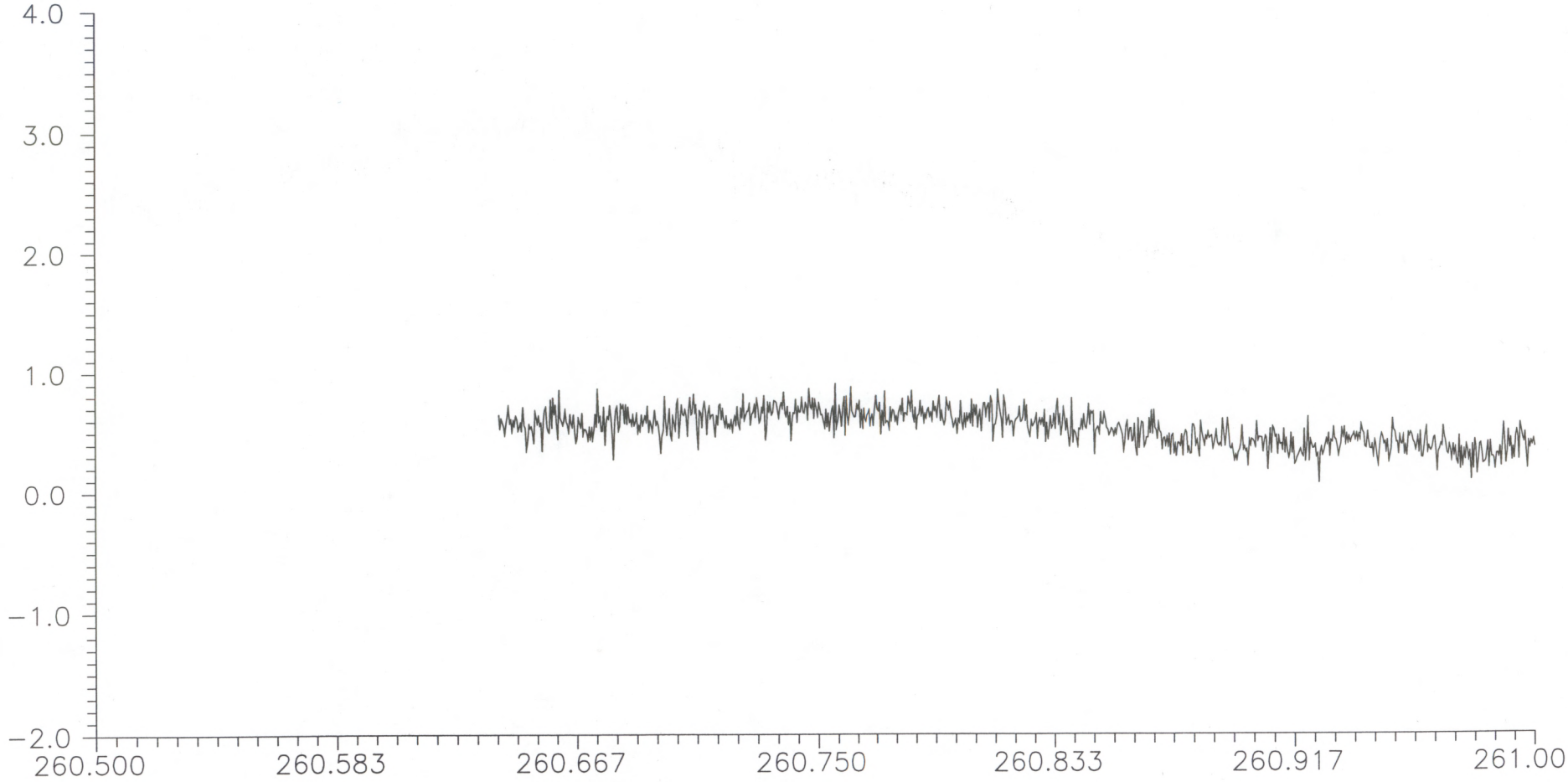

Fig. 28. Time series of 36-s averaged radiometrically-derived sea/air temperature difference.

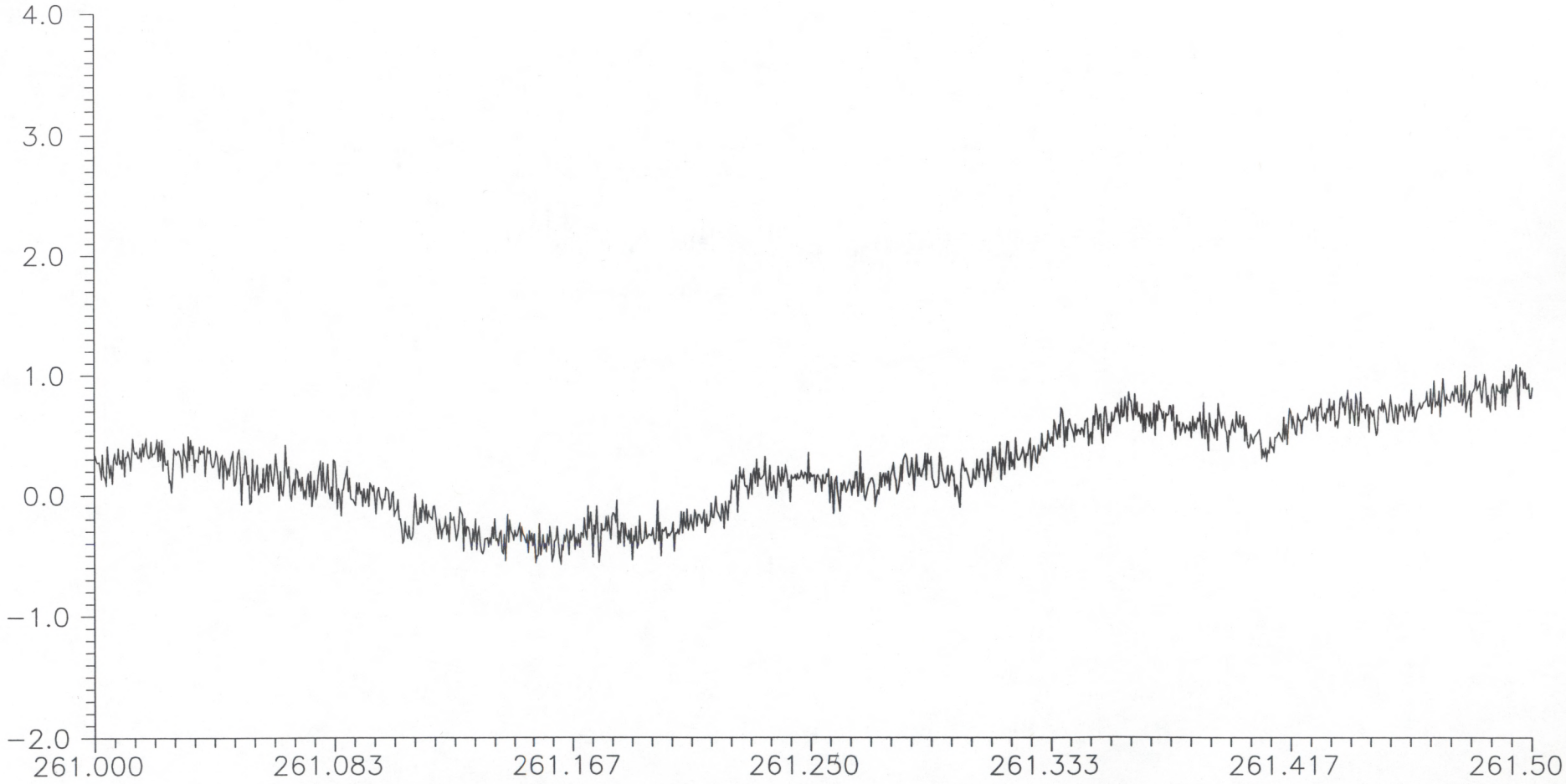

Fig. 29. Time series of 36-s averaged radiometrically-derived sea/air temperature difference.

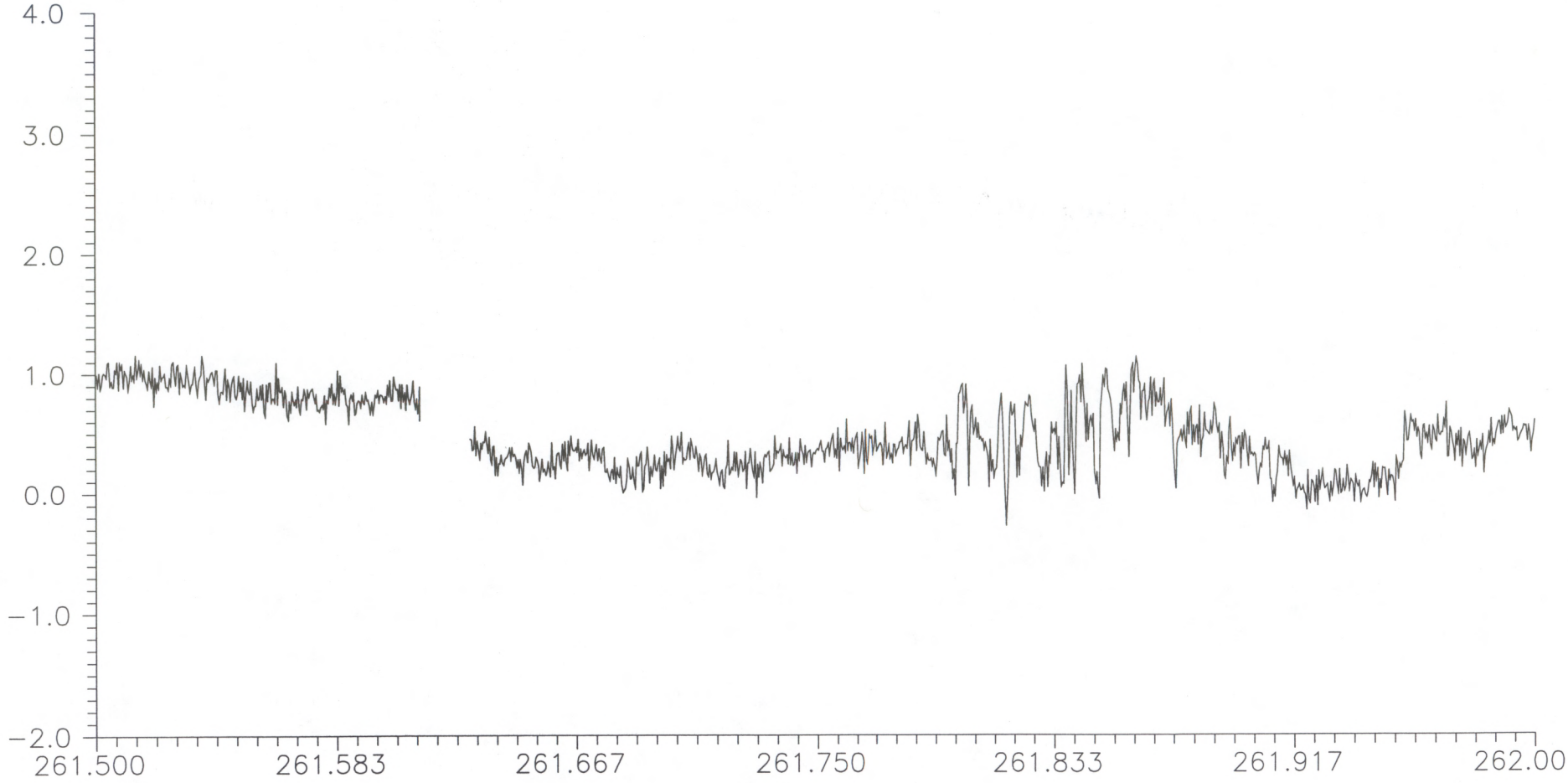

Fig. 30. Time series of 36-s averaged radiometrically-derived sea/air temperature difference.

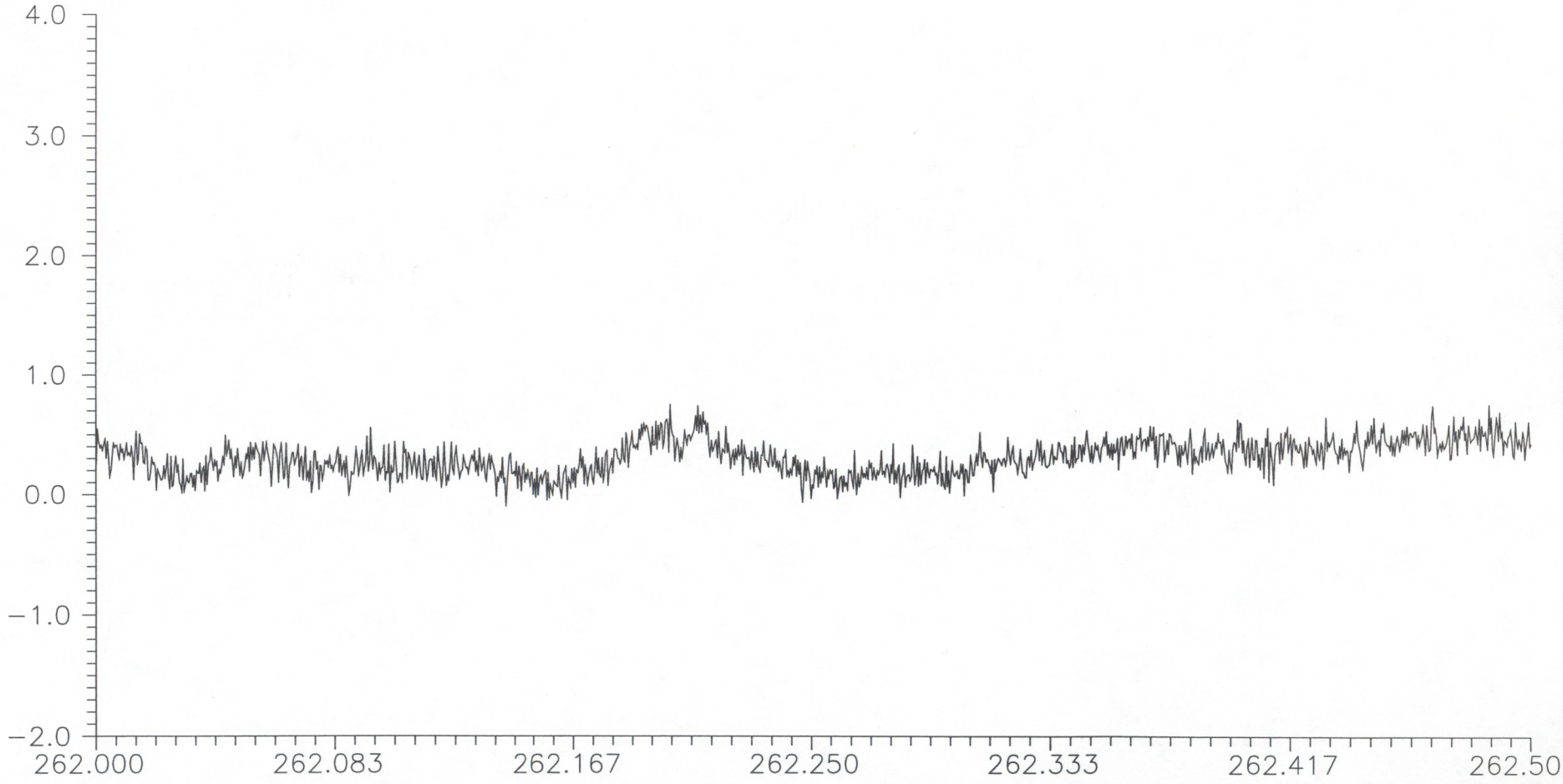

Fig. 31. Time series of 36-s averaged radiometrically-derived sea/air temperature difference.

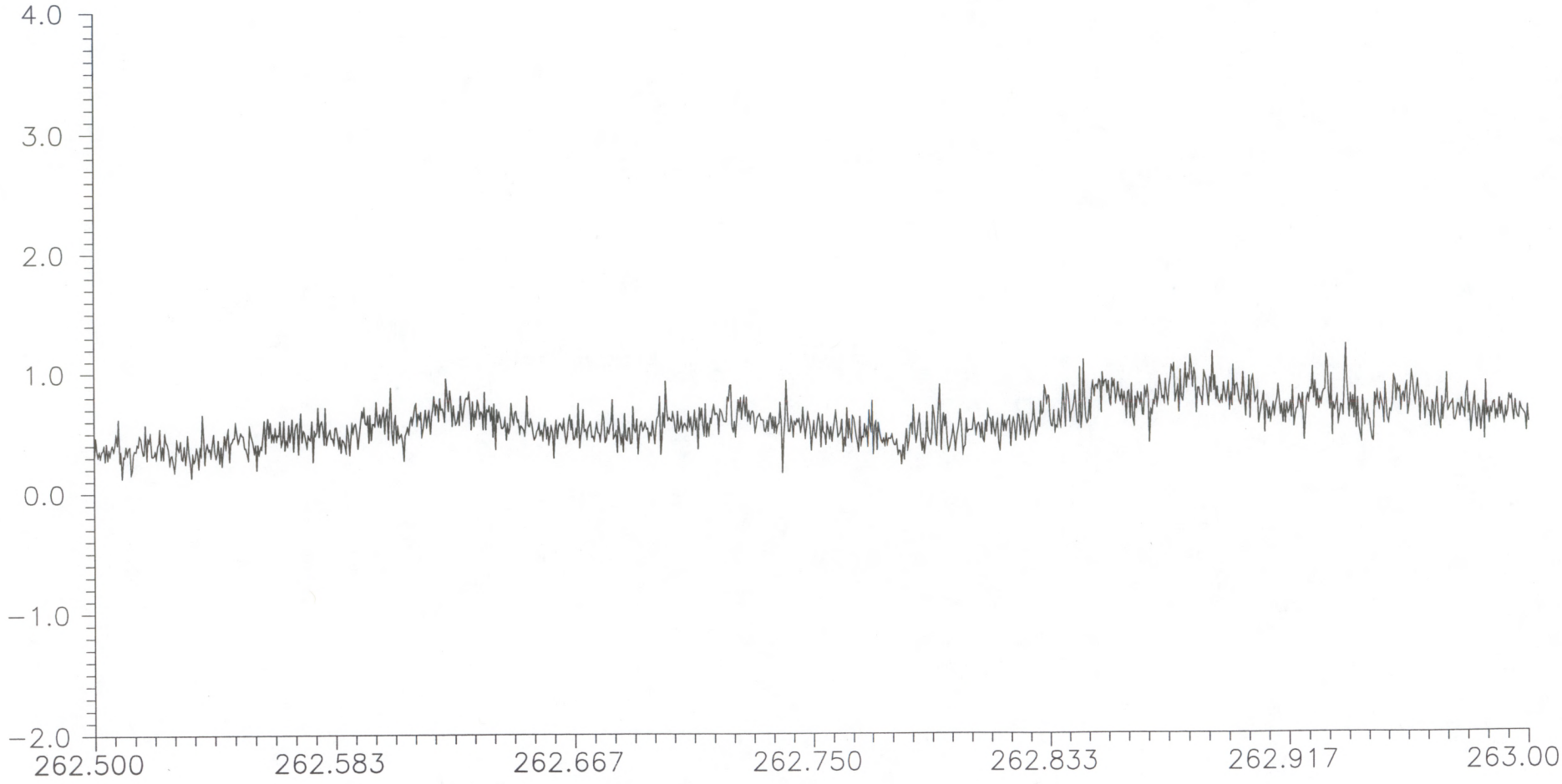

Fig. 32. Time series of 36-s averaged radiometrically-derived sea/air temperature difference.

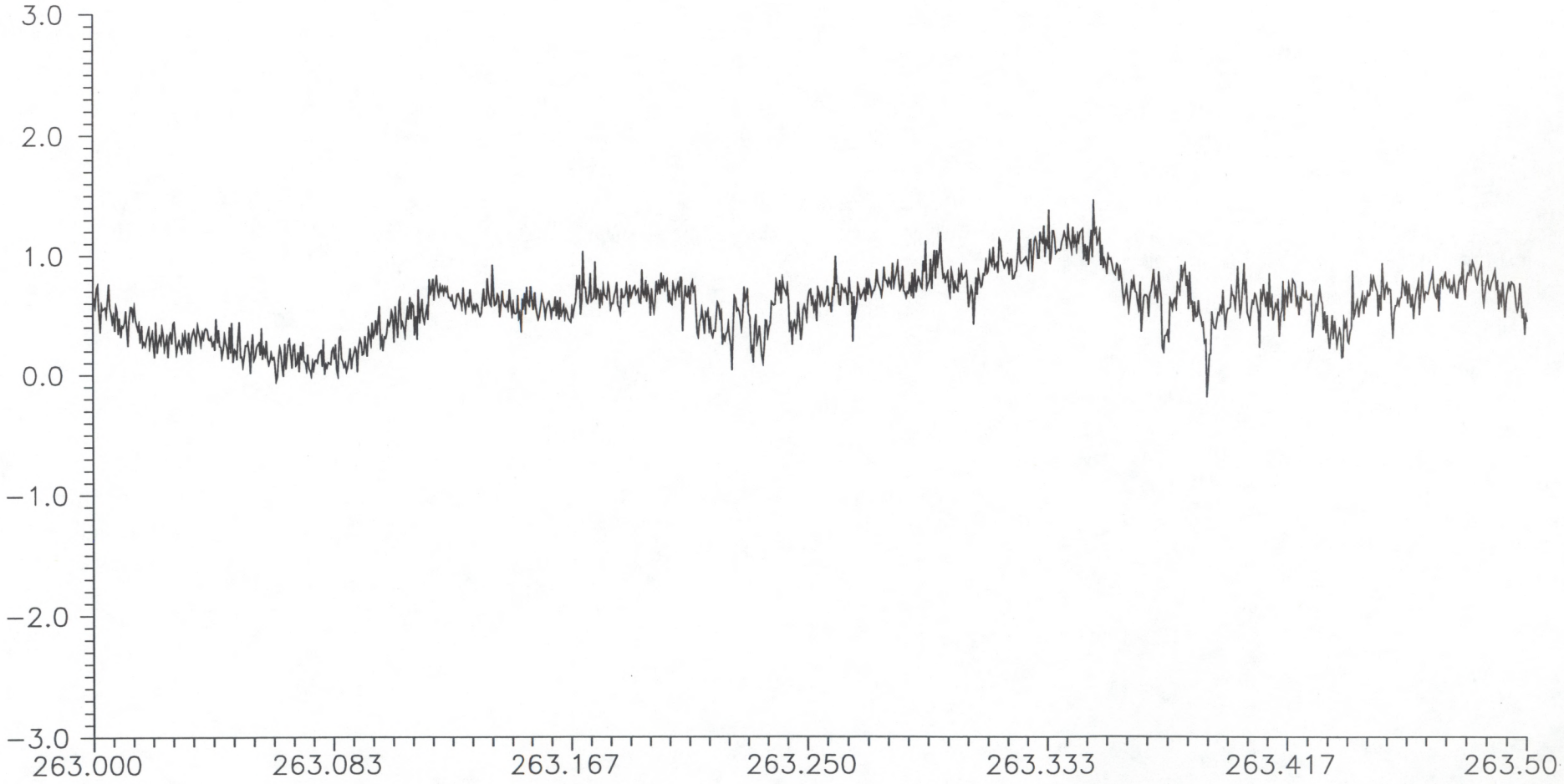

Fig. 33. Time series of 36-s averaged radiometrically-derived sea/air temperature difference.

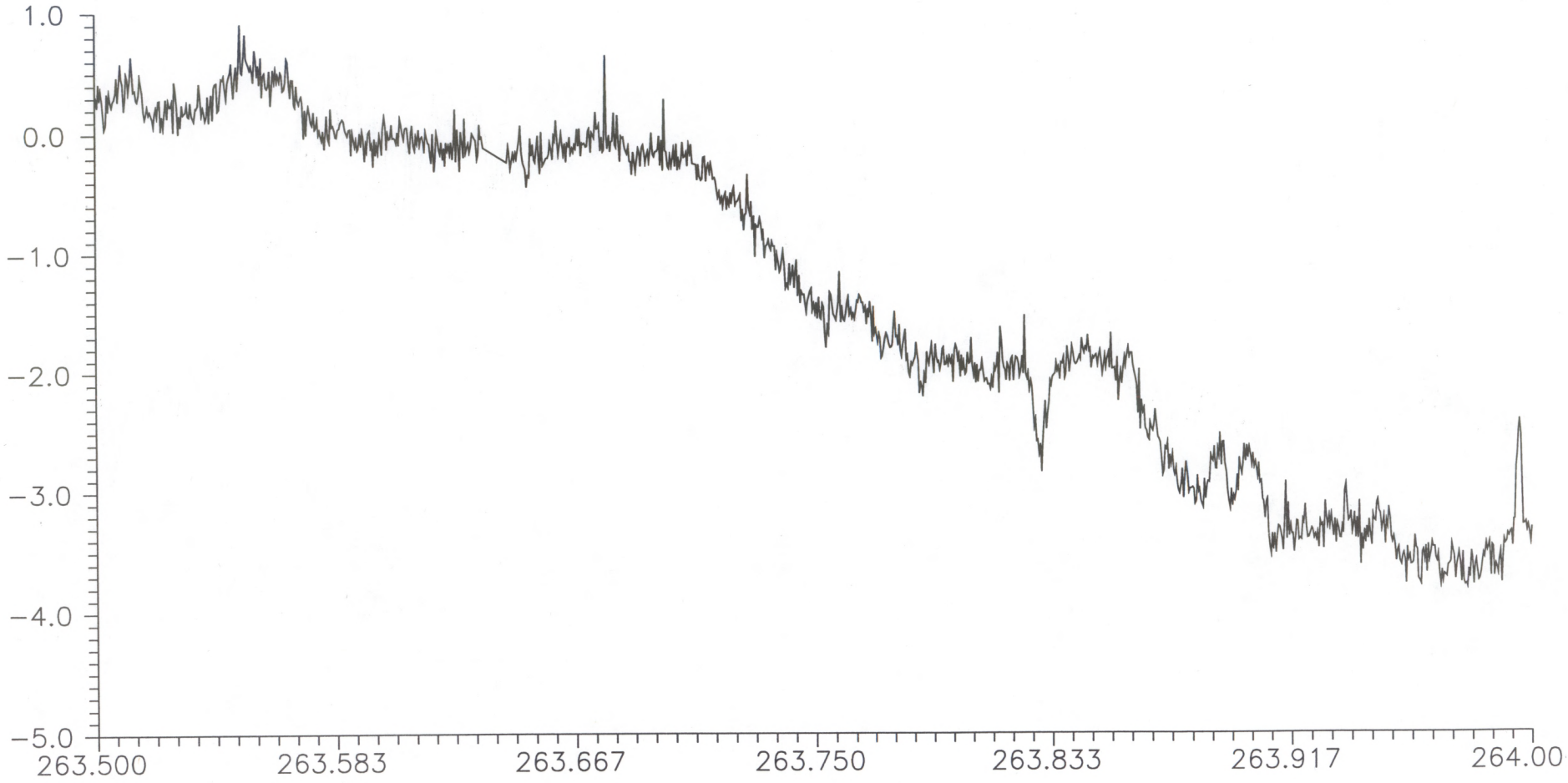

Fig. 34. Time series of 36-s averaged radiometrically-derived sea/air temperature difference.

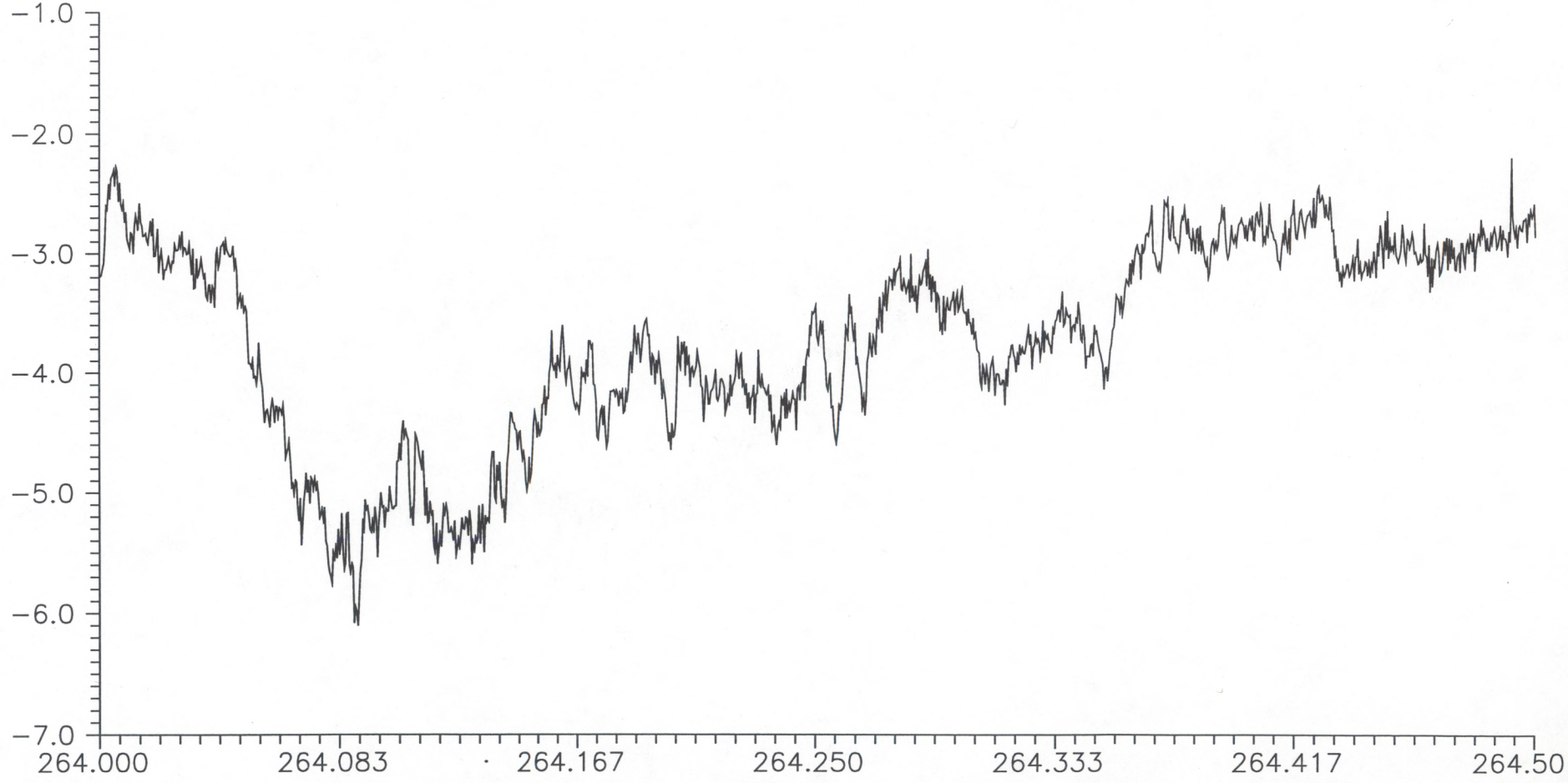

Fig. 35. Time series of 36-s averaged radiometrically-derived sea/air temperature difference.

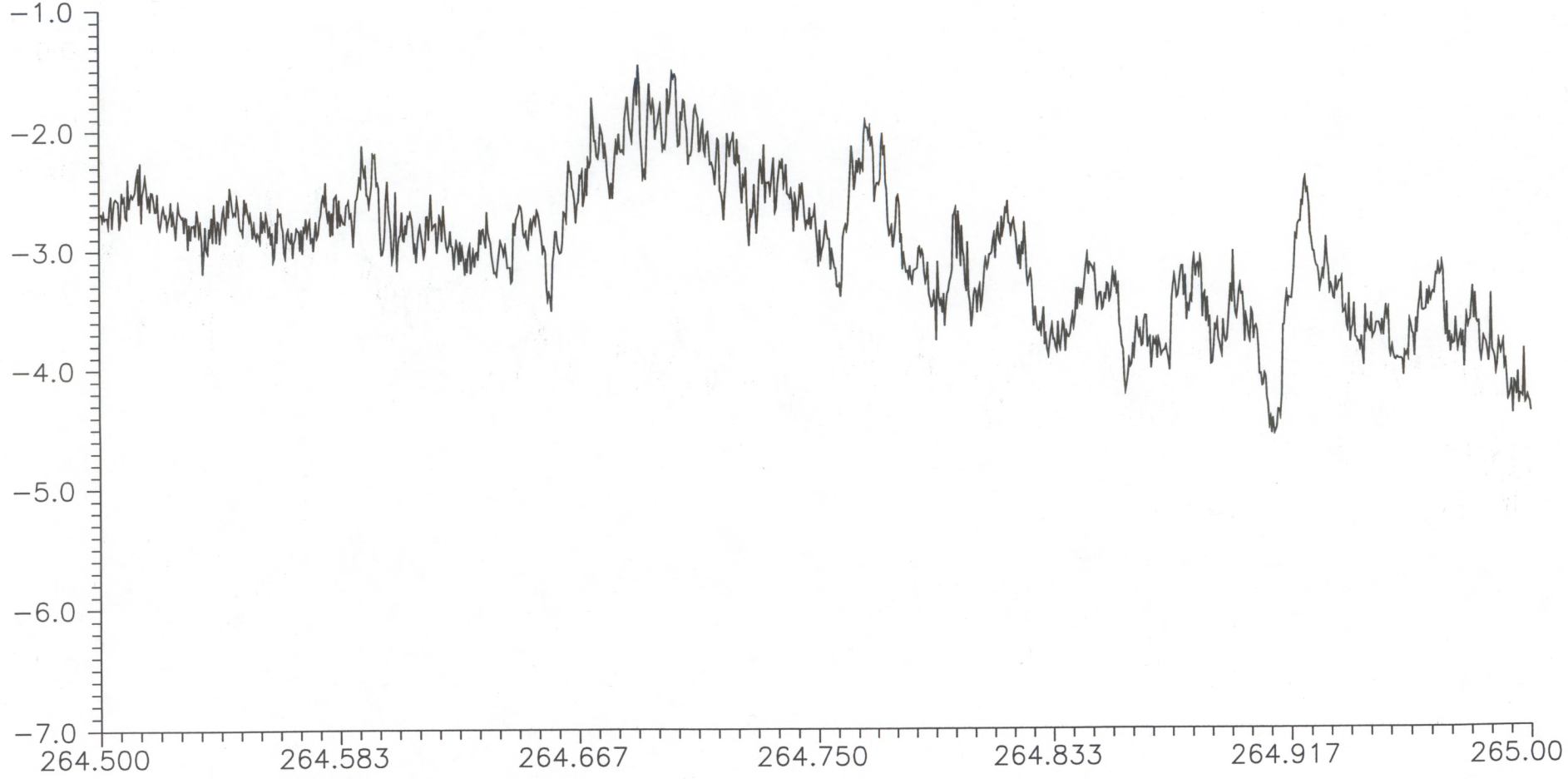

Fig. 36. Time series of 36-s averaged radiometrically-derived sea/air temperature difference.

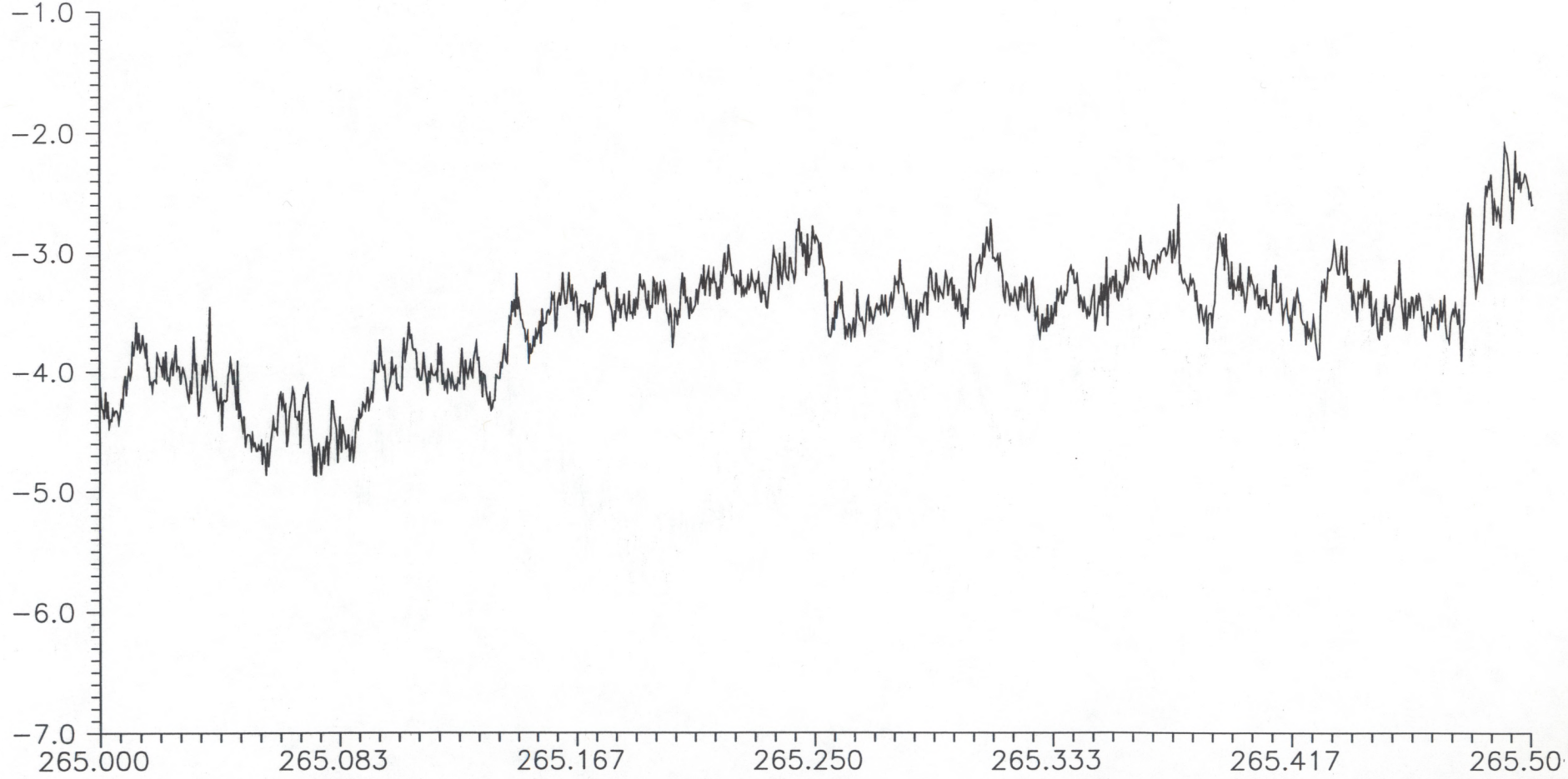

Fig. 37. Time series of 36-s averaged radiometrically-derived sea/air temperature difference.

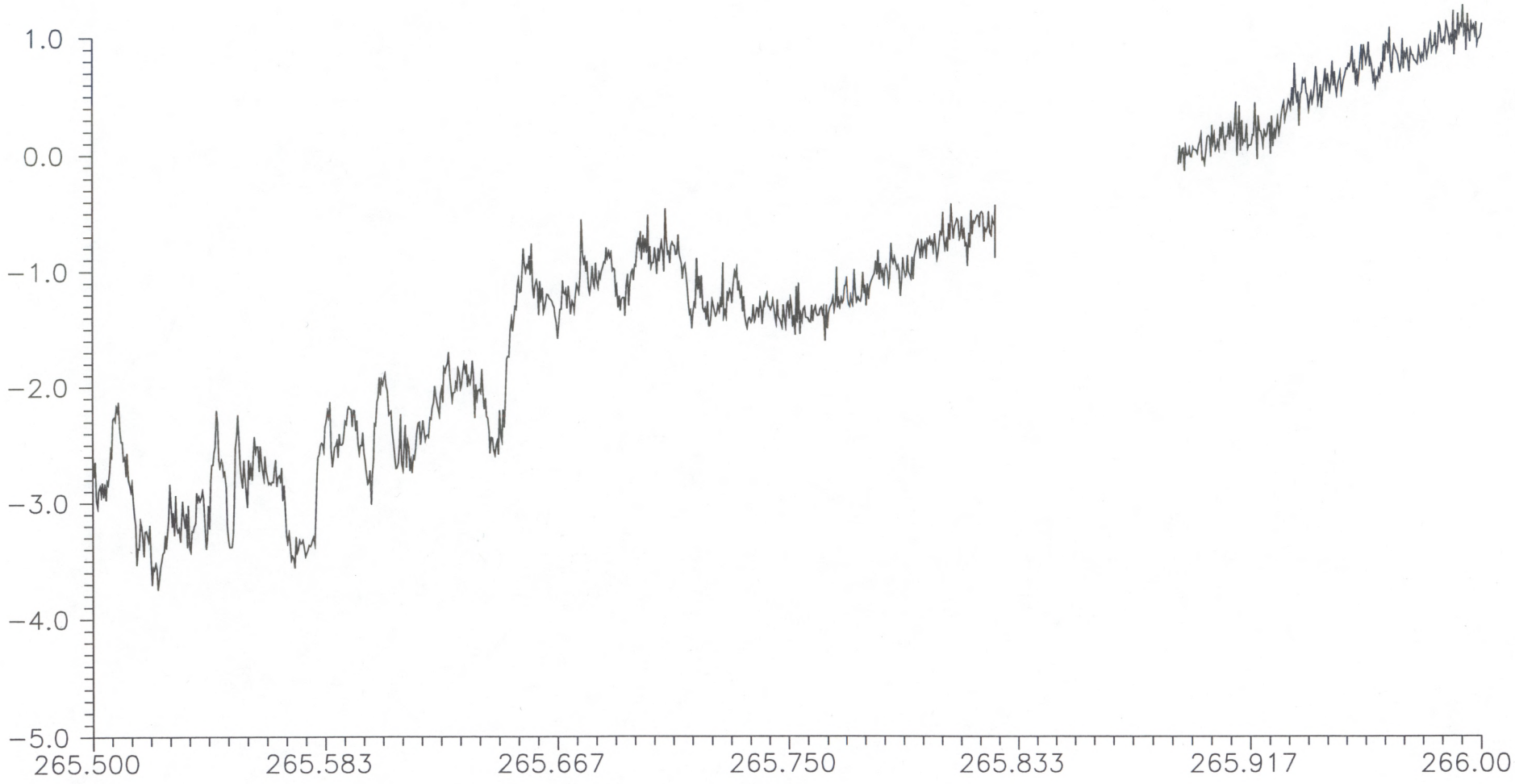

Fig. 38. Time series of 36-s averaged radiometrically-derived sea/air temperature difference.

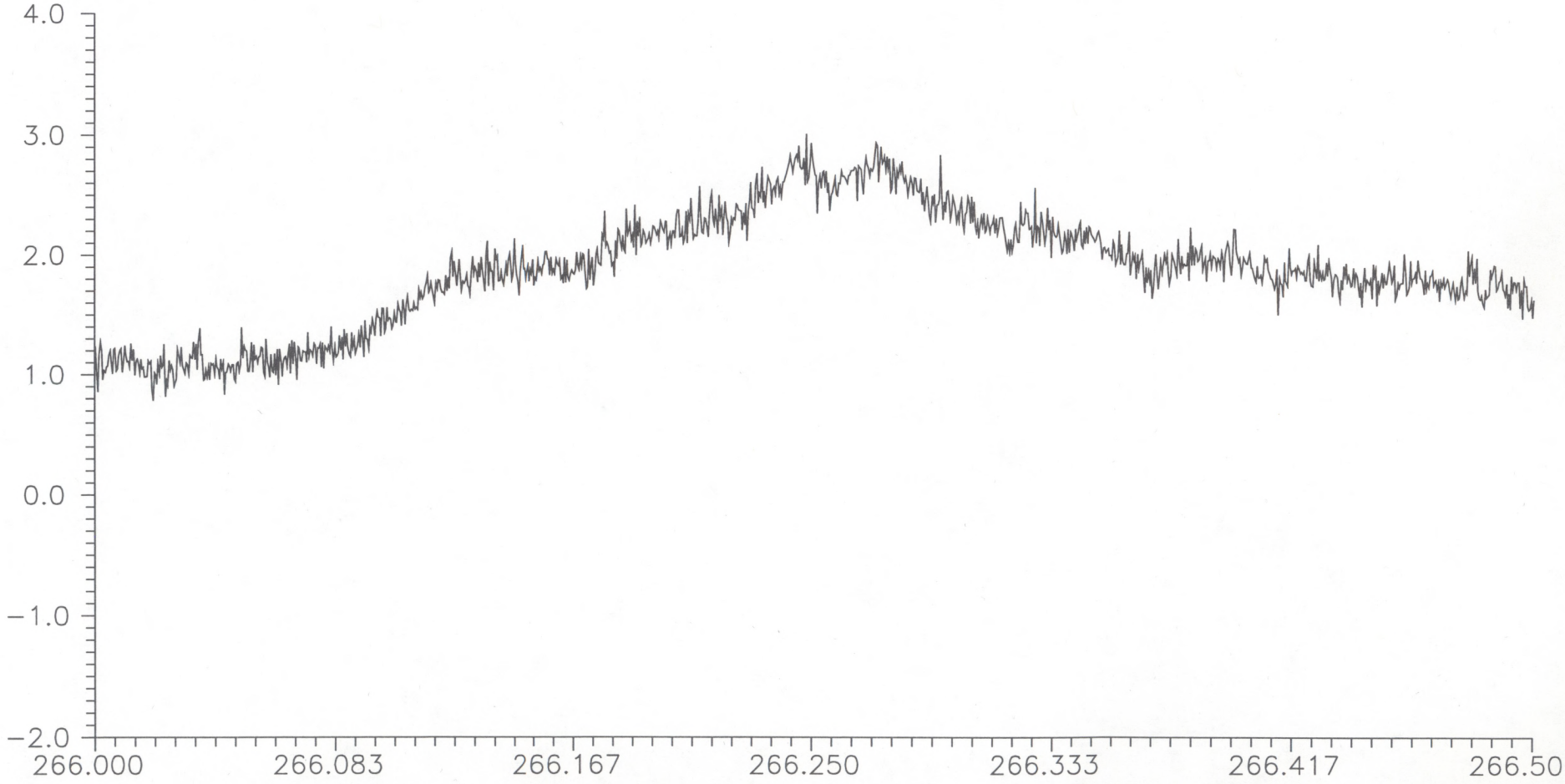

Fig. 39. Time series of 36-s averaged radiometrically-derived sea/air temperature difference.

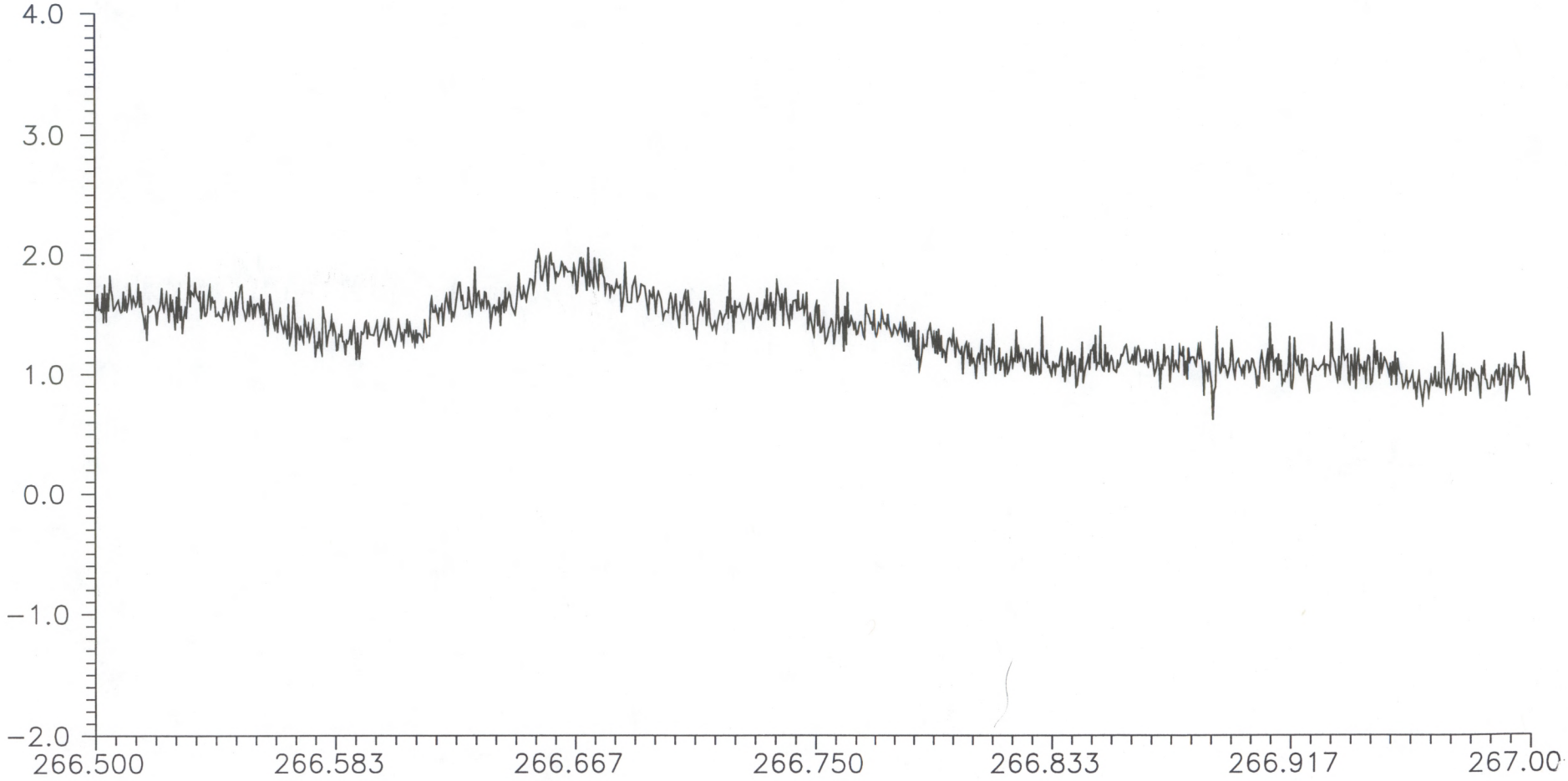

Fig. 40. Time series of 36-s averaged radiometrically-derived sea/air temperature difference.

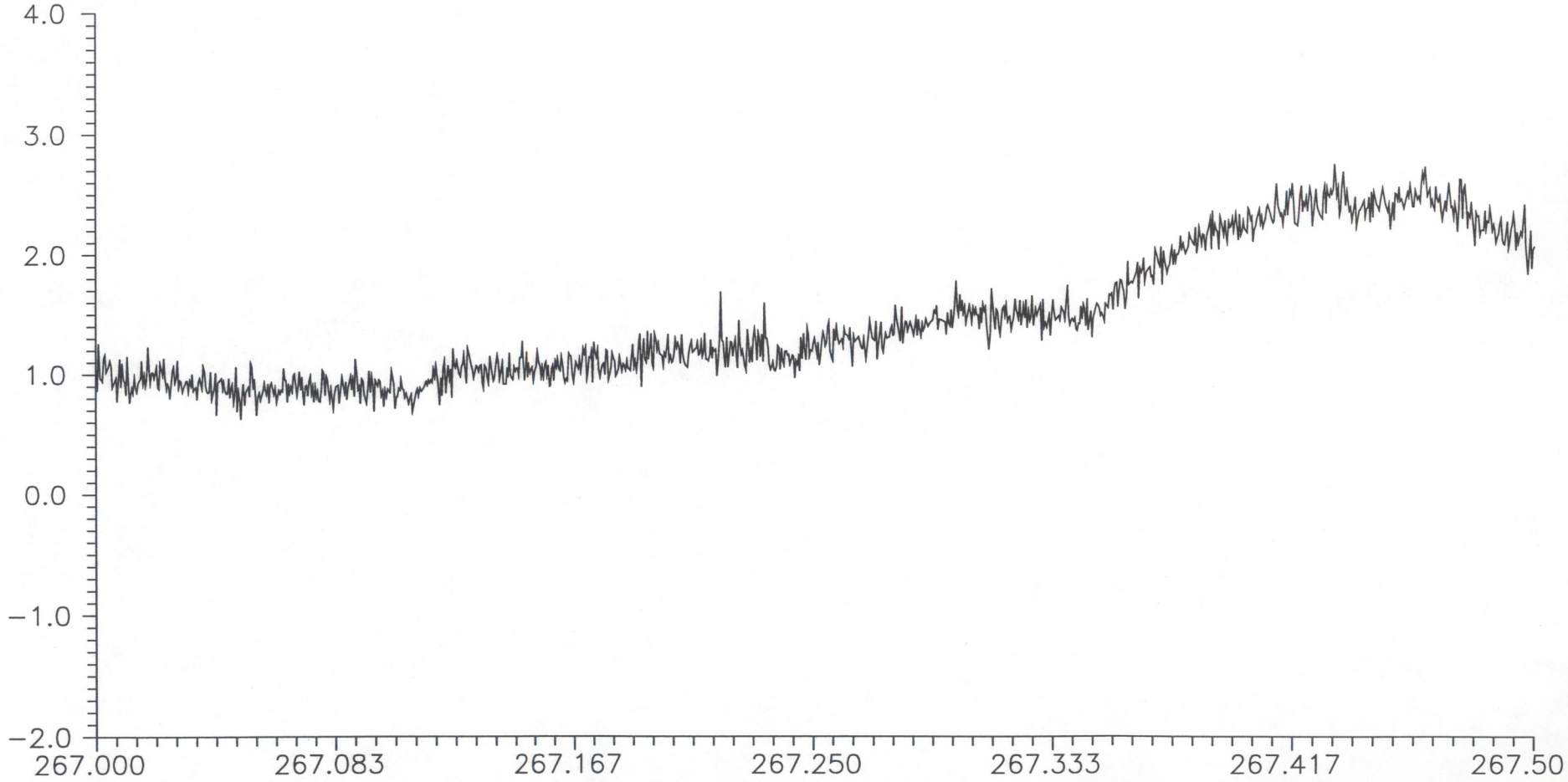

Fig. 41. Time series of 36-s averaged radiometrically-derived sea/air temperature difference.

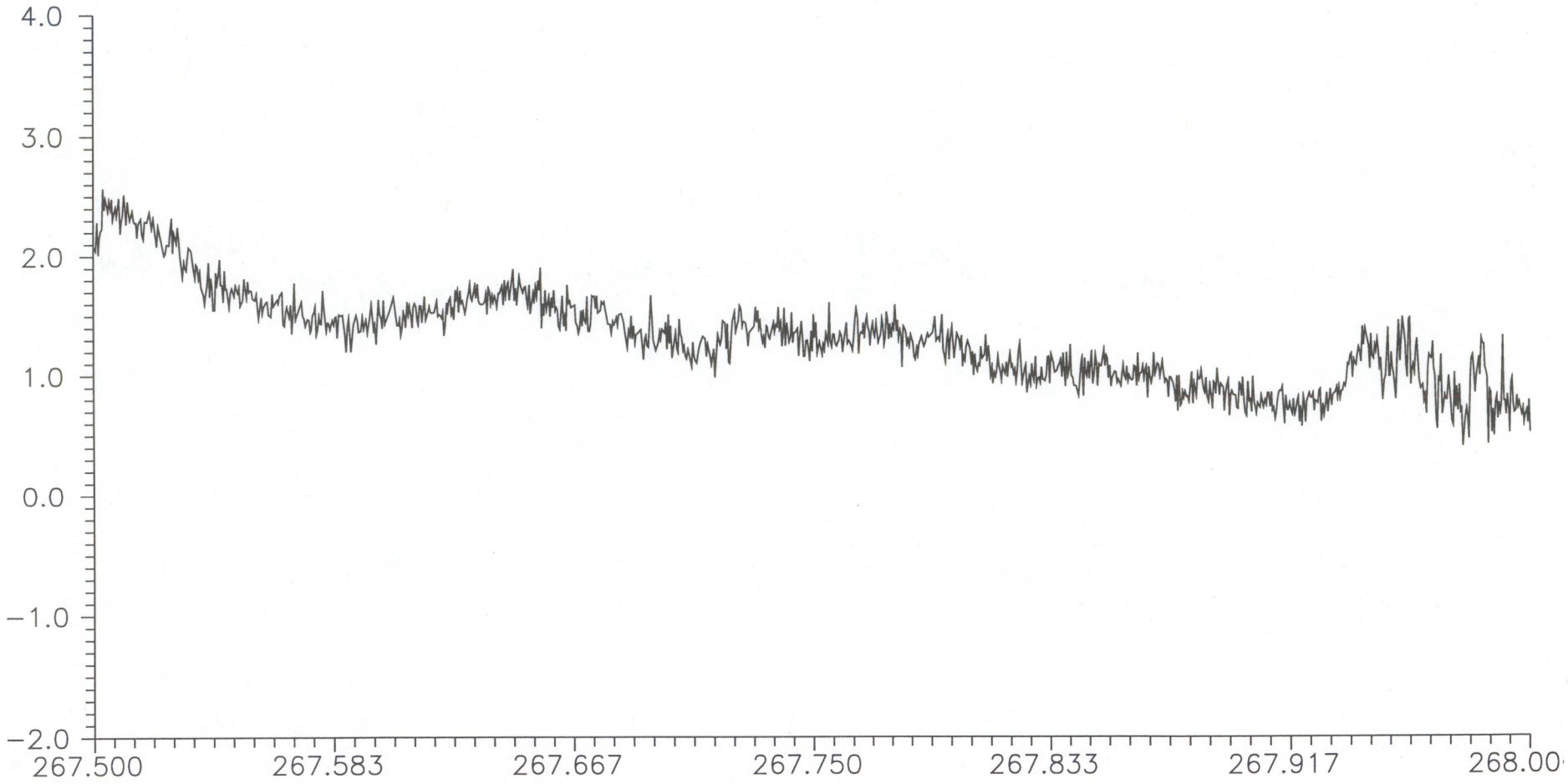

Fig. 42. Time series of 36-s averaged radiometrically-derived sea/air temperature difference.

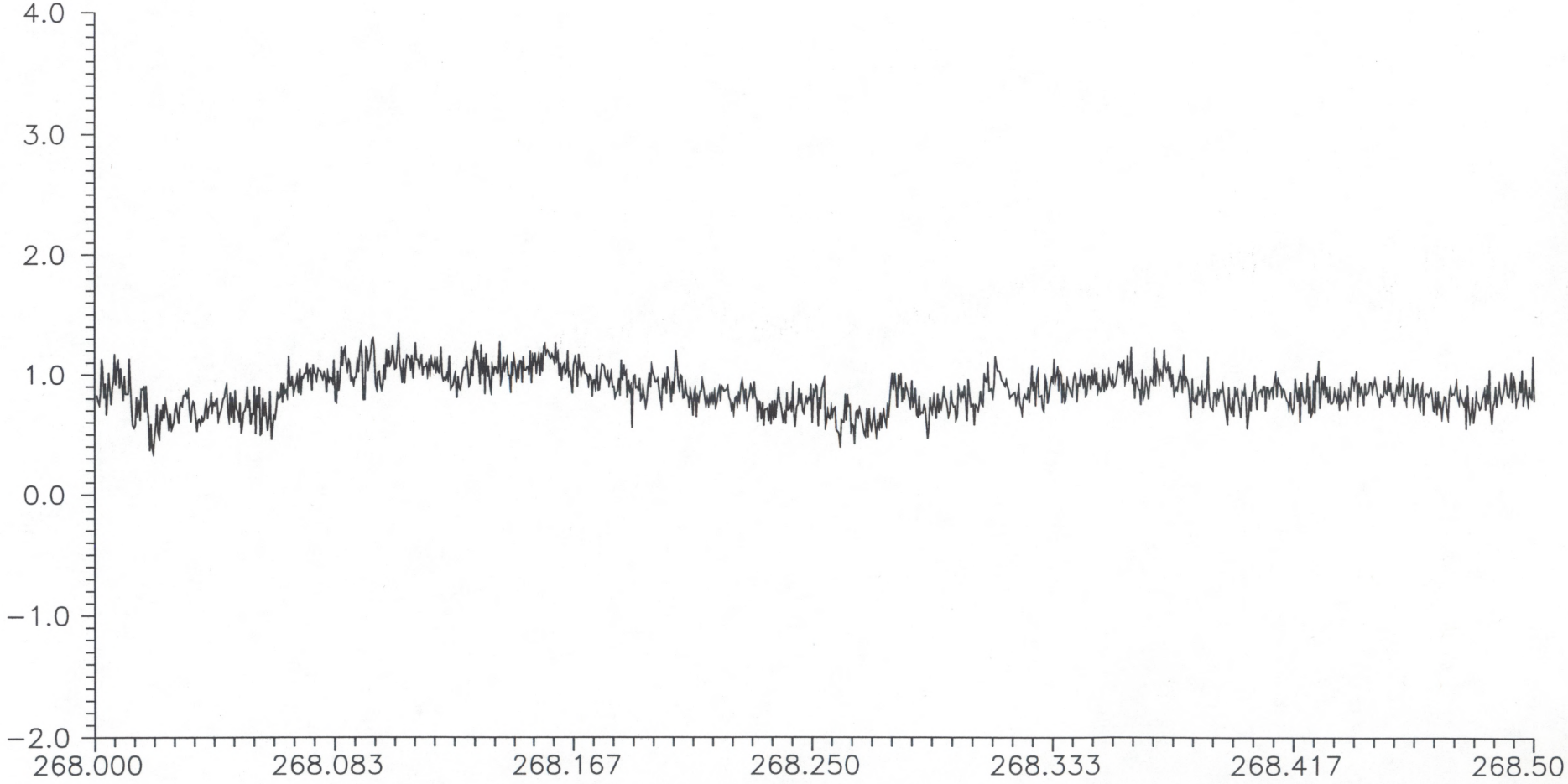

Fig. 43. Time series of 36-s averaged radiometrically-derived sea/air temperature difference.

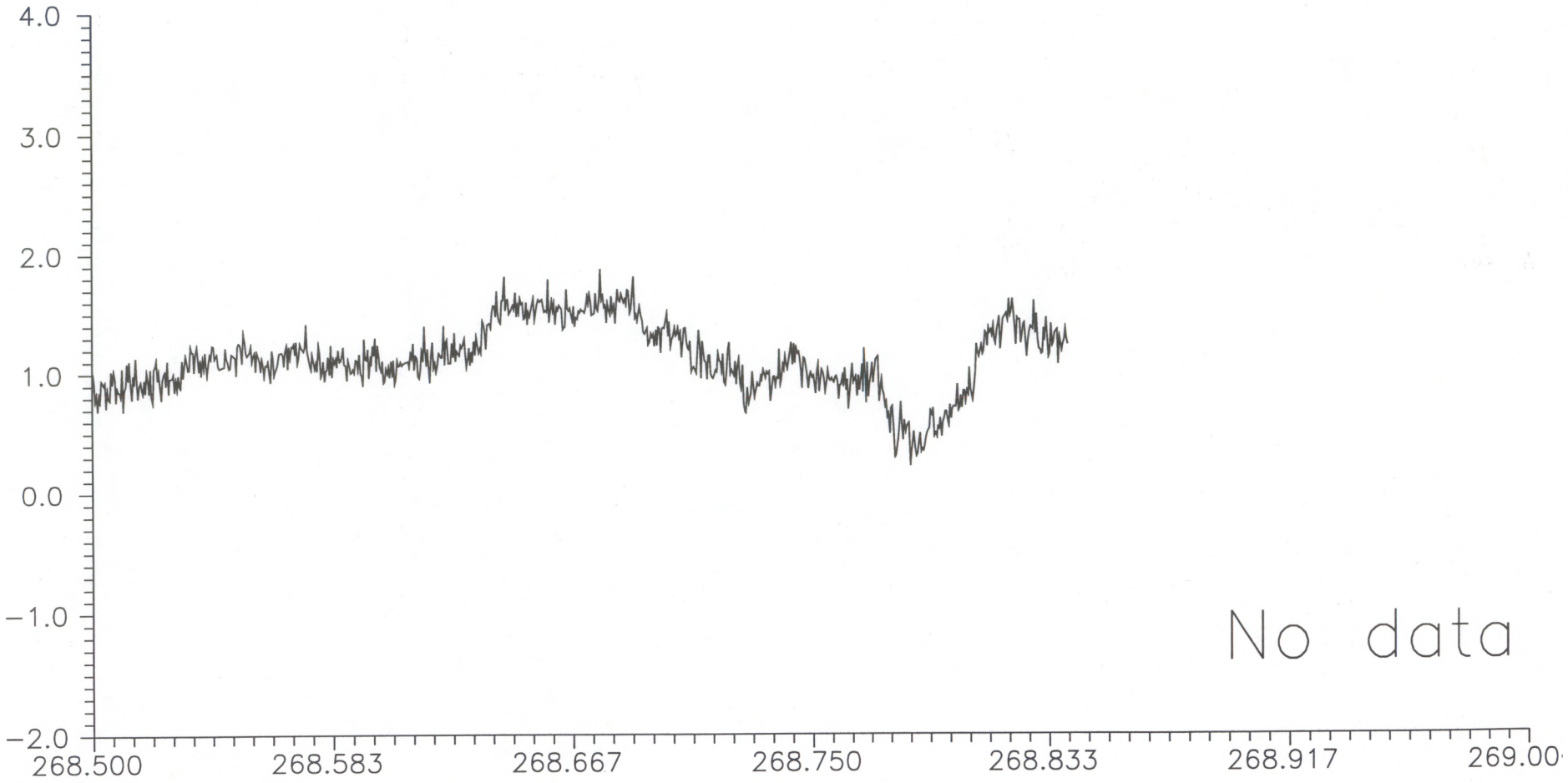

Fig. 44. Time series of 36-s averaged radiometrically-derived sea/air temperature difference.

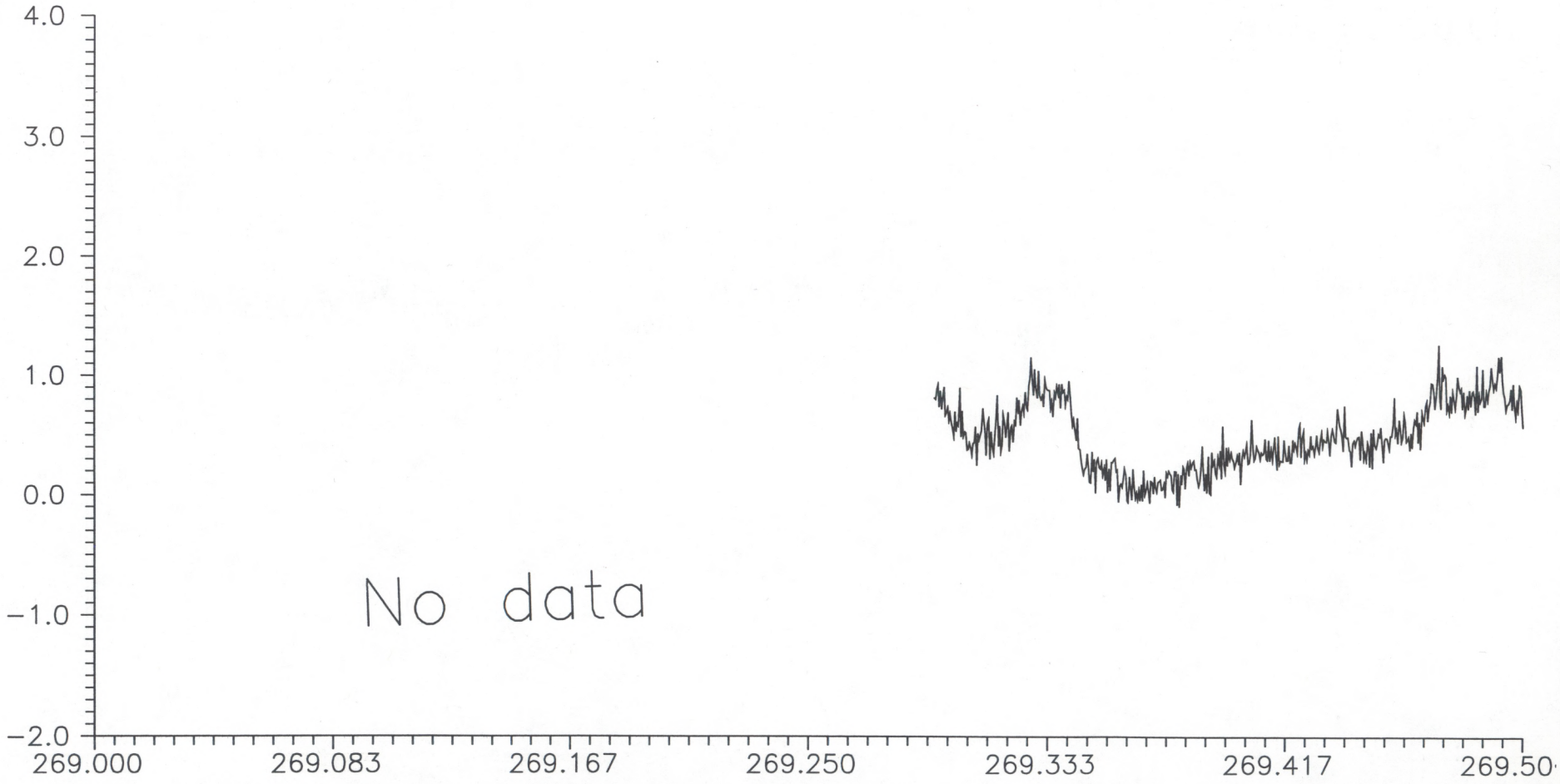

Fig. 45. Time series of 36-s averaged radiometrically-derived sea/air temperature difference.

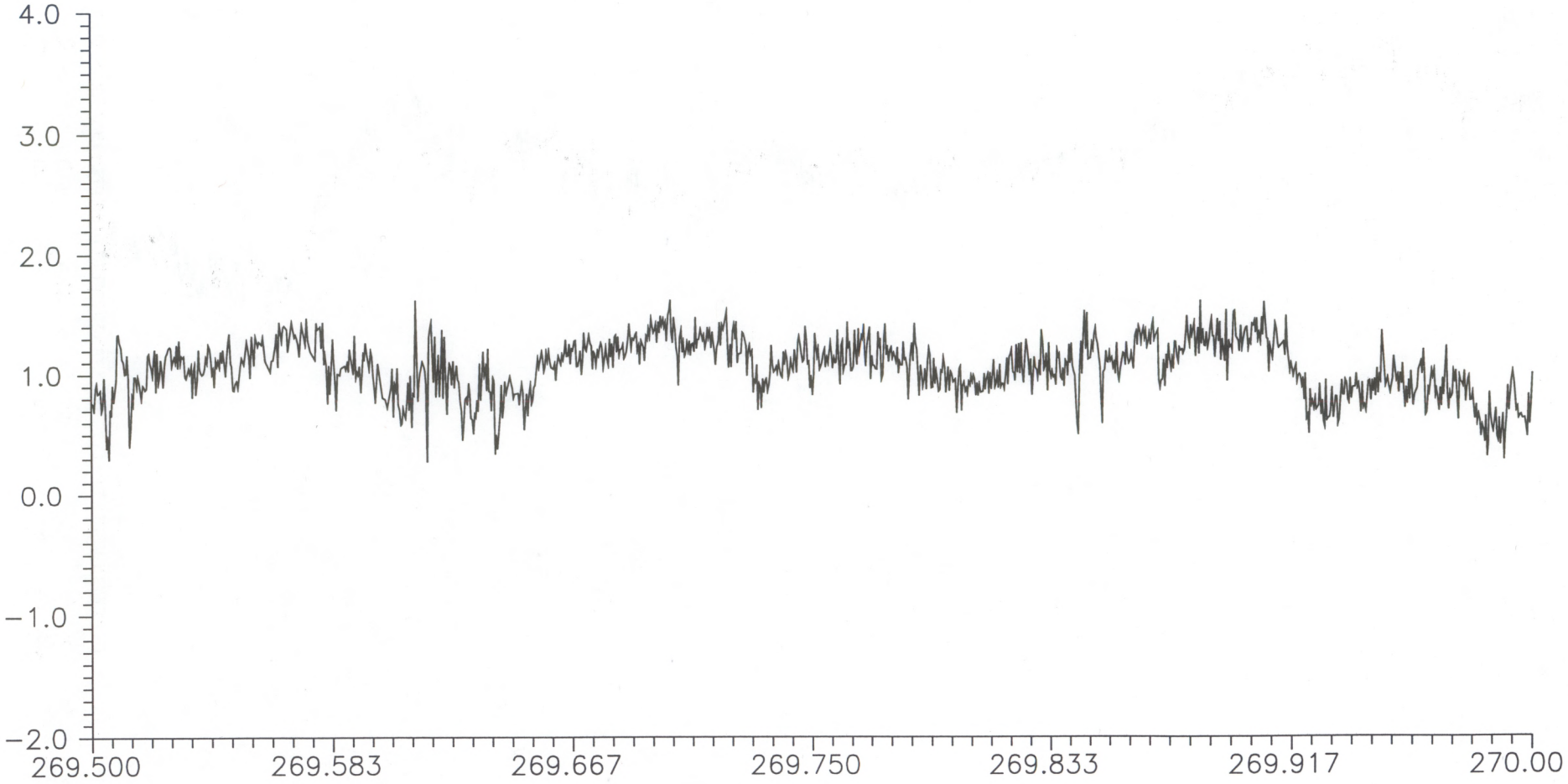

Fig. 46. Time series of 36-s averaged radiometrically-derived sea/air temperature difference.

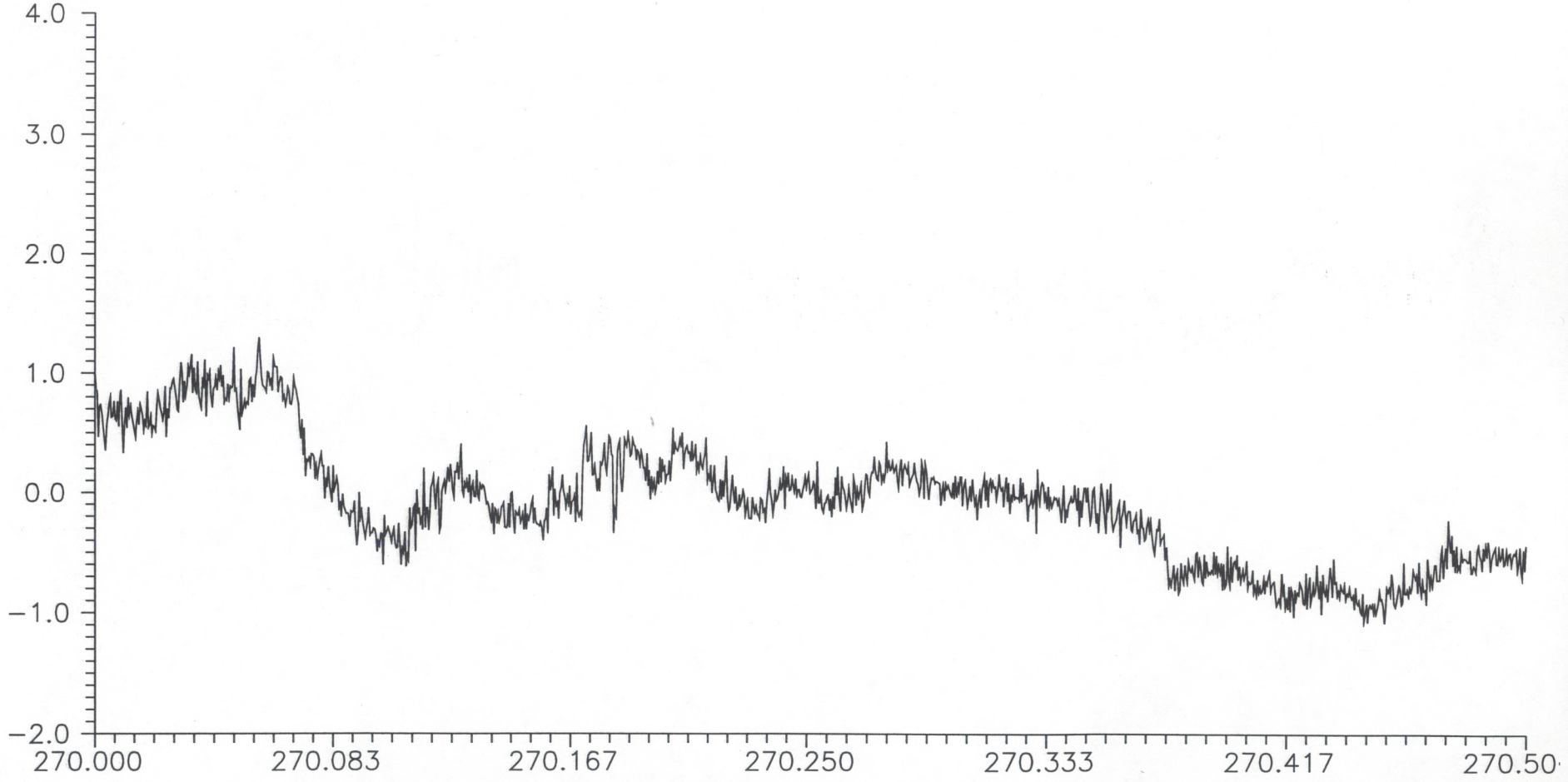

Fig. 47. Time series of 36-s averaged radiometrically-derived sea/air temperature difference.

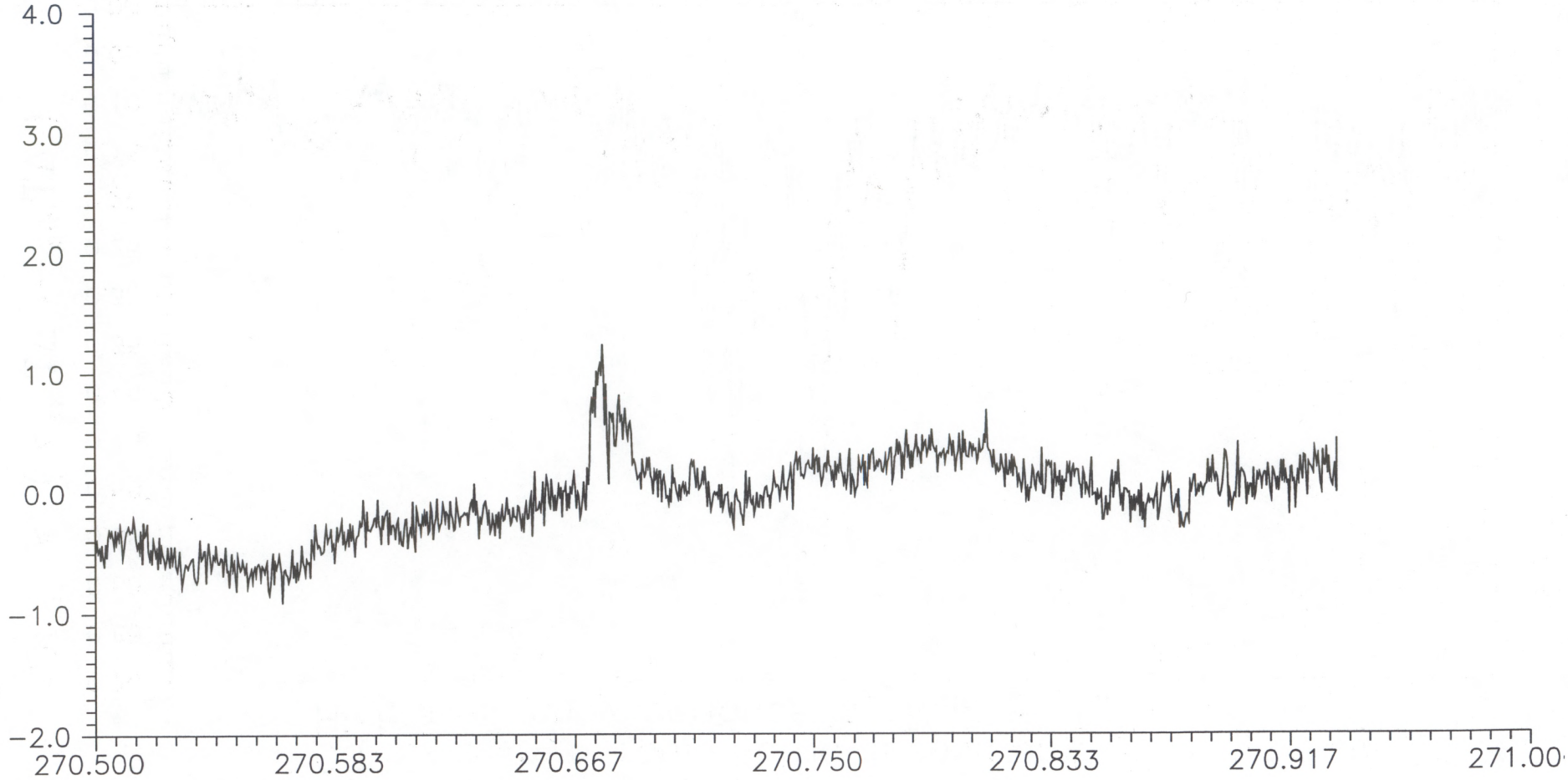

Fig. 48. Time series of 36-s averaged radiometrically-derived sea/air temperature difference.

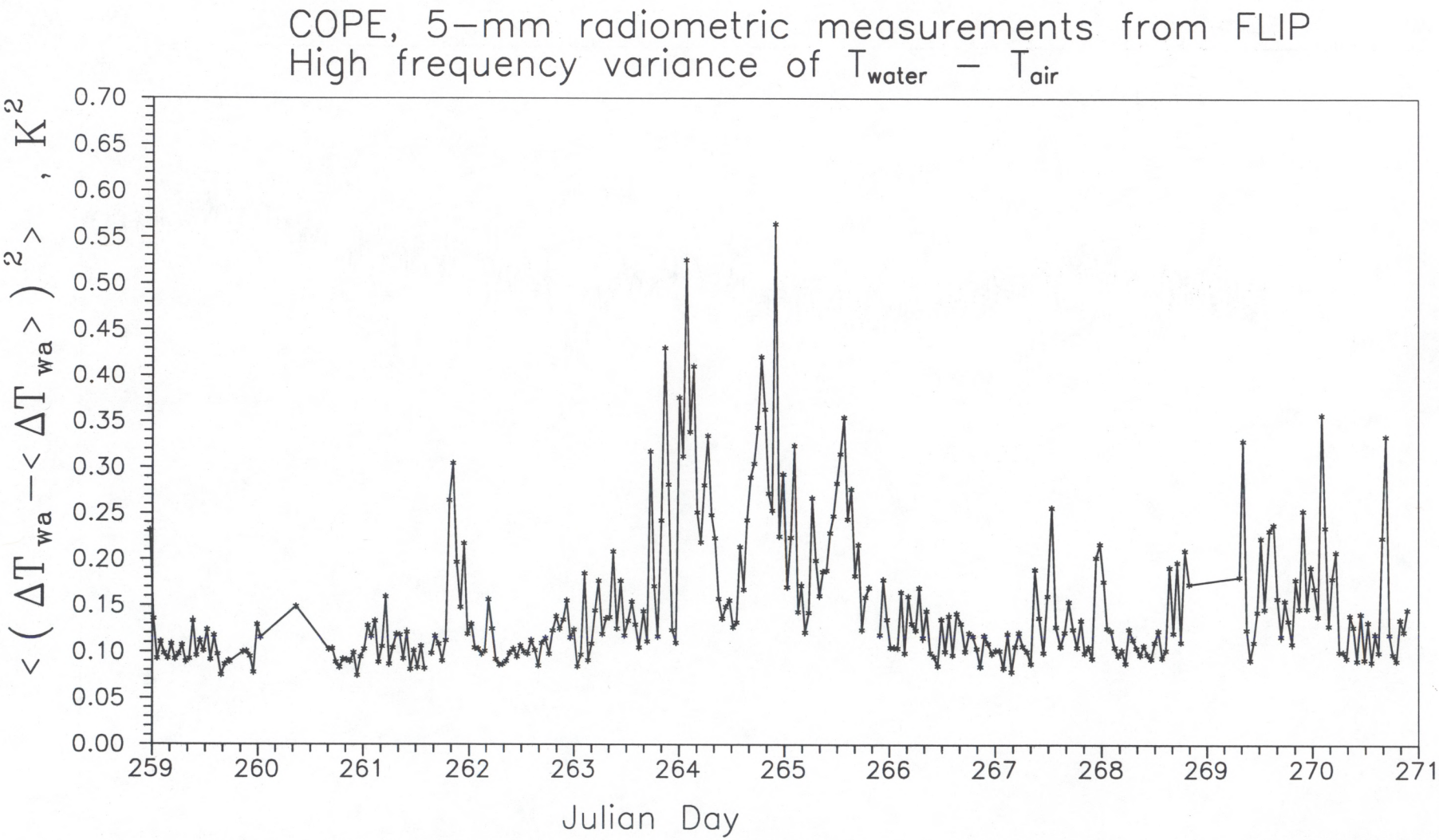

Fig. 49. Time series of high frequency variance of radiometrically-derived sea/air temperature difference.

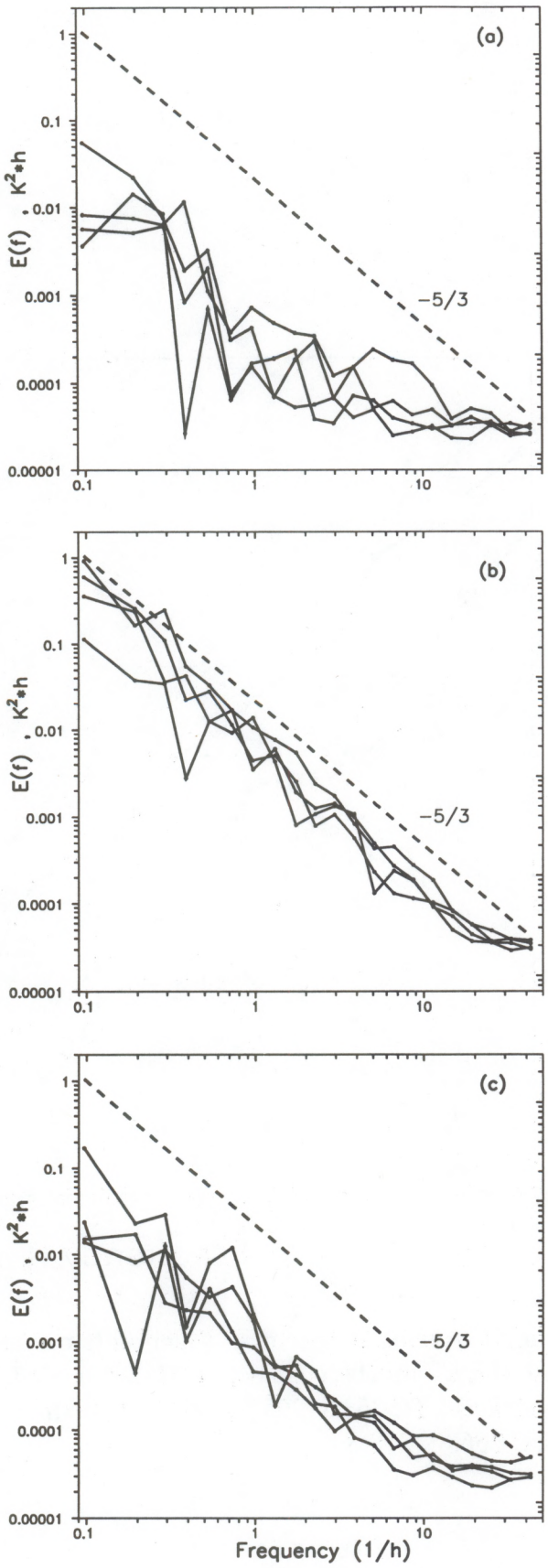

Fig. 50. Examples of spectra taken during stable and unstable conditions; each from data of 10.3 h duration: (a) unstable, (b) stable , (c) unstable.

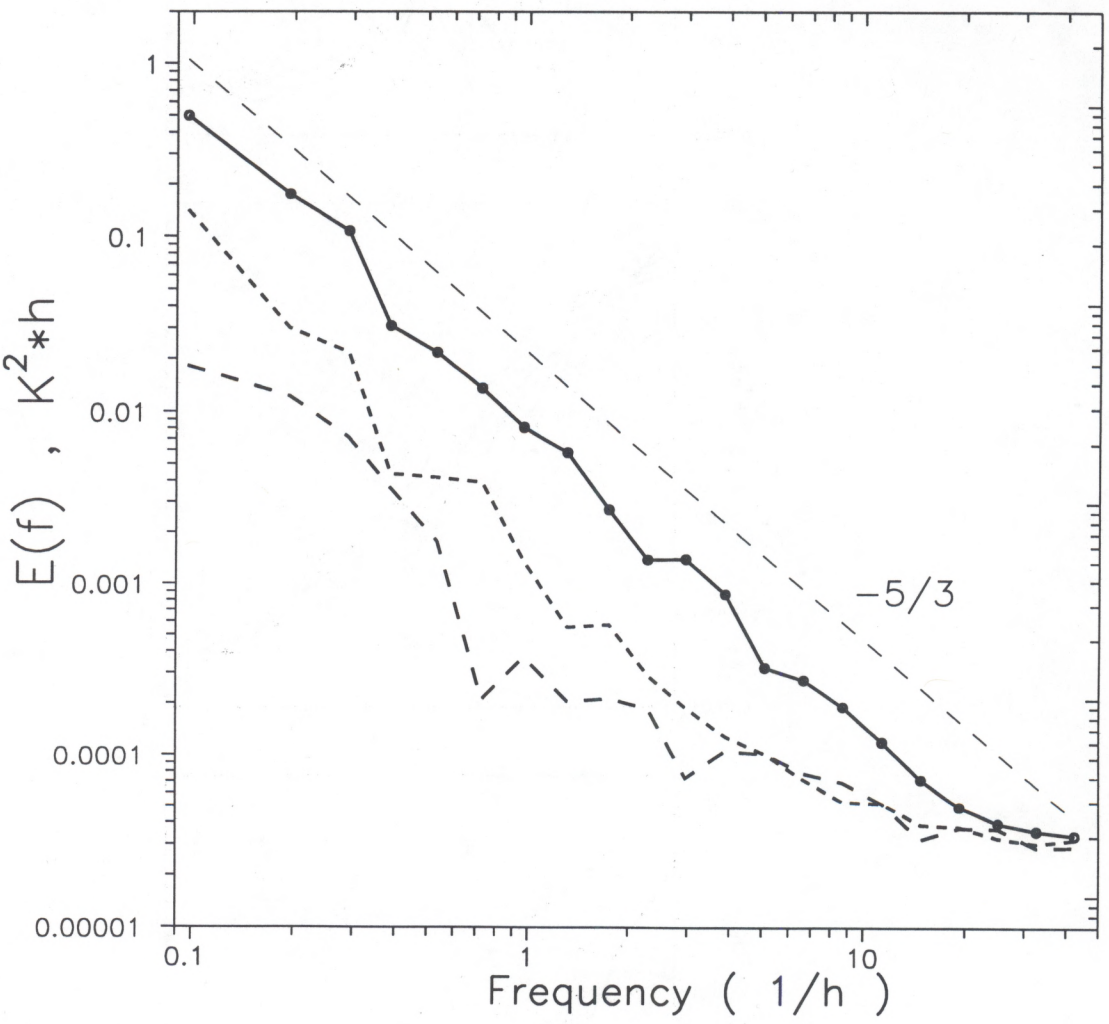

Fig. 51. Averaged spectra of water-air temperature difference. Long dashed line - unstable conditions UTC 261.6 - 263.3, sollid line - stable conditions UTC 263.8 -265.5 , short dashed line - unstable conditions UTC 266.8 - 268.5.